NGR-05-007-416

UCLA-ENG-7546
JUNE 1975

(NASA-CR-143111) INTERACTIONS OF SATELLITE-SPEED HELIUM ATOMS WITH SATELLITE-SURFACES. 1: SPATIAL DISTRIBUTIONS OF REFLECTED HELIUM ATOMS (California Univ.) 43 p HC $3.75 CSCL 20H G3/72

N75-27874

Unclas
29212

INTERACTIONS OF SATELLITE-SPEED HELIUM ATOMS WITH SATELLITE-SURFACES
I: SPATIAL DISTRIBUTIONS OF REFLECTED HELIUM ATOMS

S.M. LIU
W.E. RODGERS
E.L. KNUTH

UCLA • SCHOOL OF ENGINEERING AND APPLIED SCIENCE

UCLA-ENG-7546
JUNE 1975

INTERACTIONS OF SATELLITE-SPEED HELIUM ATOMS WITH SATELLITE SURFACES

I: SPATIAL DISTRIBUTIONS OF REFLECTED HELIUM ATOMS

by

S. M. Liu
W. E. Rodgers
E. L. Knuth

School of Engineering and Applied Science
University of California
Los Angeles, California

FOREWORD

The researches described here were supported mainly by the National Aeronautics and Space Administration (under Grant NGR 05-007-416) and by the UCLA School of Engineering and Applied Science. These studies were part of a continuing program of researches in gas-surface interactions.

ABSTRACT

Interactions of satellite-speed helium atoms with practical satellite surfaces have been investigated experimentally. Spatial distributions of satellite-speed helium beams scattered from four different engineering surfaces were measured. The 7000 m/sec helium beams were produced using an arc-heated supersonic molecular beam source. The test surfaces included cleaned 6061-T6 aluminum plate, anodized aluminum foil, white paint and quartz surfaces. Both in-plane (i.e., in the plane containing the incident beam and the surface normal) and out-of-plane spatial distributions of reflected helium atoms were measured for six different incidence angles (0°, 15°, 30°, 45°, 60°, and 75° from the surface normal). It was found that a large fraction of the incident helium atoms were scattered back in the vicinity of the incoming beam, particularly in the case of glancing incidence angles. This unexpected scattering feature results perhaps from the gross roughness of these test surfaces. This prominent backscattering could yield drag coefficients which are higher than for surfaces with either forward-lobed or diffusive (cosine) scattering patterns.

TABLE OF CONTENTS

Page

LIST OF FIGURES

Figure | Page

Figure | Page

LIST OF SYMBOLS

$\hat{n}$	surface normal
$\hat{t}$	surface tangent
θ_i	incidence angle of helium atom measured from surface normal
θ_r	in-plane scattering angle measured from surface normal
ϕ	out-of-plane scattering angle measured from the plane of incidence

CHAPTER I

INTRODUCTION

The aerodynamic drag experienced by an earth satellite in the upper atmosphere can be investigated in a laboratory environment using an ultra-high vacuum system and the molecular beam technique. The desired information concerning the momentum accommodation (therefore, the drag coefficient) can be extracted from the change in the molecular beam properties during the surface collision if the states of the incident beam and the scattered beam (spatial density distribution and speed distribution) are completely determined. This report presents results of the first part (i.e., the spatial distributions) of a two-part experimental study of interactions of satellite-speed helium atoms with satellite surfaces.

Scattering distributions of high-energy molecular beams from solid surfaces have been measured by several authors [1-6]. However, most of these distributions were measured with relatively smooth single-crystal metal surfaces and heavy inert atoms. Also, all these measurements were confined to the plane of incidence. These measured scattering distributions were single-lobed and peaked near the specular direction; the signal-to-noise ratios were relatively large. In the case of a helium beam scattered from a practical satellite surface, one would expect a relatively diffusive scattering distribution and a relatively weak scattered-beam signal-to-noise ratio.

In Chapter II, the experimental apparatus and procedures are described briefly. Experimental results and related discussions are given in Chapter III.

CHAPTER II

EXPERIMENTAL APPARATUS AND PROCEDURES

The present experimental study was carried out in the UCLA Molecular-Beam Laboratory. The molecular beam system used for the present work has been described in detail by Hays [7] and by Liu [8]. Hence it will be described only briefly here. Figure II-1 shows a schematic diagram of the molecular-beam system. The satellite-speed (7000 m/sec) helium beams were generated by an arc-heated supersonic beam source developed by Young [9]. The incident beam was collimated by a collimating orifice of 0.10-inch diameter placed between the collimation chamber and the detection chamber. The nickle-plated detection chamber was pumped by a 10-inch oil-diffusion pump and a liquid-nitrogen cryopump. The background pressure in the detection chamber was 1×10^{-7} Torr (composed mostly of nitrogen and oxygen residual gases) under normal operating conditions.

A new mechanism, shown in Figure II-2, was constructed for facilitating both in-plane and out-of-plane scattering-distribution measurements. This new mechanism includes (1) a target holder and its positioning mechanism and (2) a detection rotating mechanism. The target holder can be rotated and moved vertically by means of a gear controlled by external feed-throughs. This two-dimensional motion facilitates varying the incidence angle under operational vacuum. Furthermore, with the target out of the beam path, the incident beam can be easily detected by the mass spectrometer. The target positioning mechanism is mounted on a base ring which is fastened to the detection chamber. The detector rotating mechanism consists of (1) a rotating ring, set on the base ring with three stainless steel balls riding in opposing grooves and driven by a low-speed motor via a positive-drive belt;

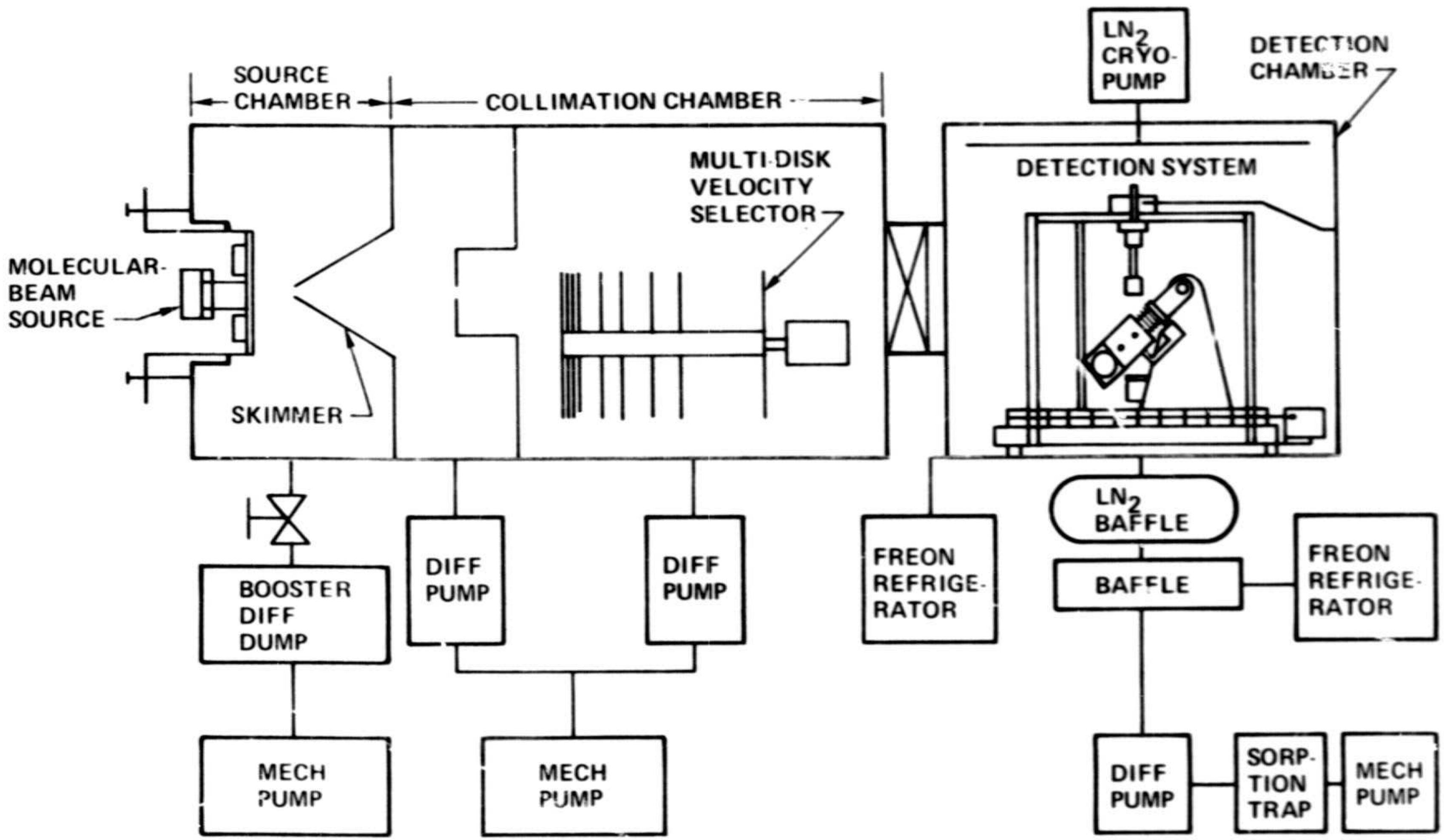

Figure II-1. Schematic Diagram of the Molecular Beam System

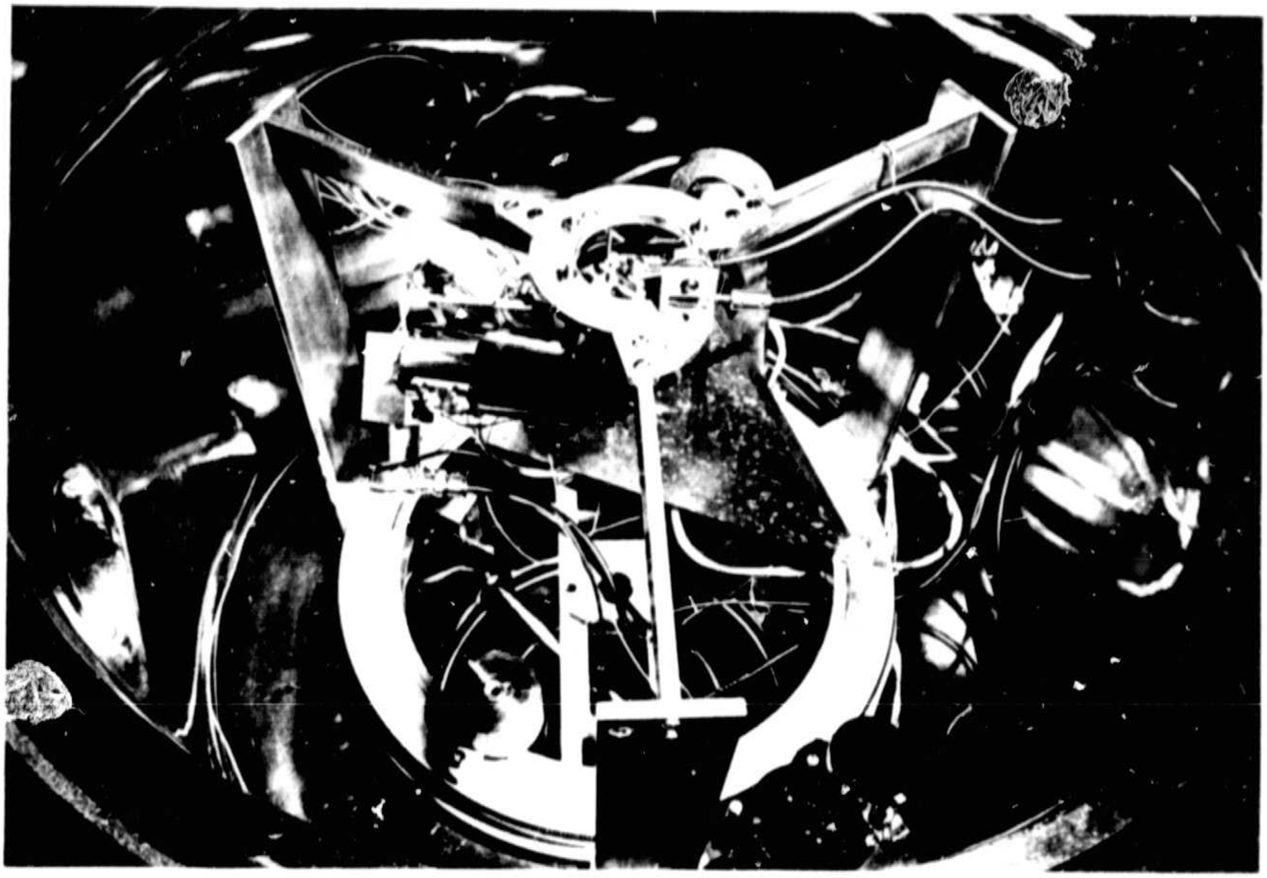

Figure II-2. Photograph of Target Assembly and Detector Sweeping Mechanism.

and (2) a gear assembly fastened to the rotating ring and also driven by a low-speed motor. The in-plane scattering (θ_r) of the detector is controlled by the rotating ring whereas the out-of-plane scattering angle (ϕ) is controlled by the gear assembly. Two 10-turn potentiometers were used to indicate the angular positions of the detector.

The detector consists of a beam chopper, an electron-bombardment ionizer, a 3-inch quadrupole mass filter, an electron multiplier, and an electronic system as shown in Figure II-3. The mass-spectrometer ionizer, with a 0.094-inch diameter inlet orifice, was placed 2 inches from the target surface. The angular resolution was approximately 3° for this configuration.

The test surfaces used in this study included (a) a cleaned 6061-T6 aluminum plate, (b) an anodized aluminum foil, (c) a white-paint surface and (d) a quartz surface. These surfaces were samples of typical satellite surfaces supplied by NASA. The aluminum foil and painted surfaces were framed with thin stainless steel plates to minimize surface distortions. All test surfaces were kept at room temperature throughout the experiments.

The scattering distributions for a helium beam impinging on a target surface with a given incidence angle were obtained by rotating the detector to a desired in-plane scattering angle (θ_r) and then sweeping the detector through 90° of out-of-plane scattering angle (ϕ). See Figure II-4. The reflected beam was first modulated by a chopper and then ionized and detected by the mass-spectrometer; the resulting signal was preamplified by a low-noise amplifier and then processed by a phase-sensitive lock-in amplifier. The outputs of the detector positioning potentiometer and the lock-in amplifier were recorded by an x-y recorder. The incident beam was characterized

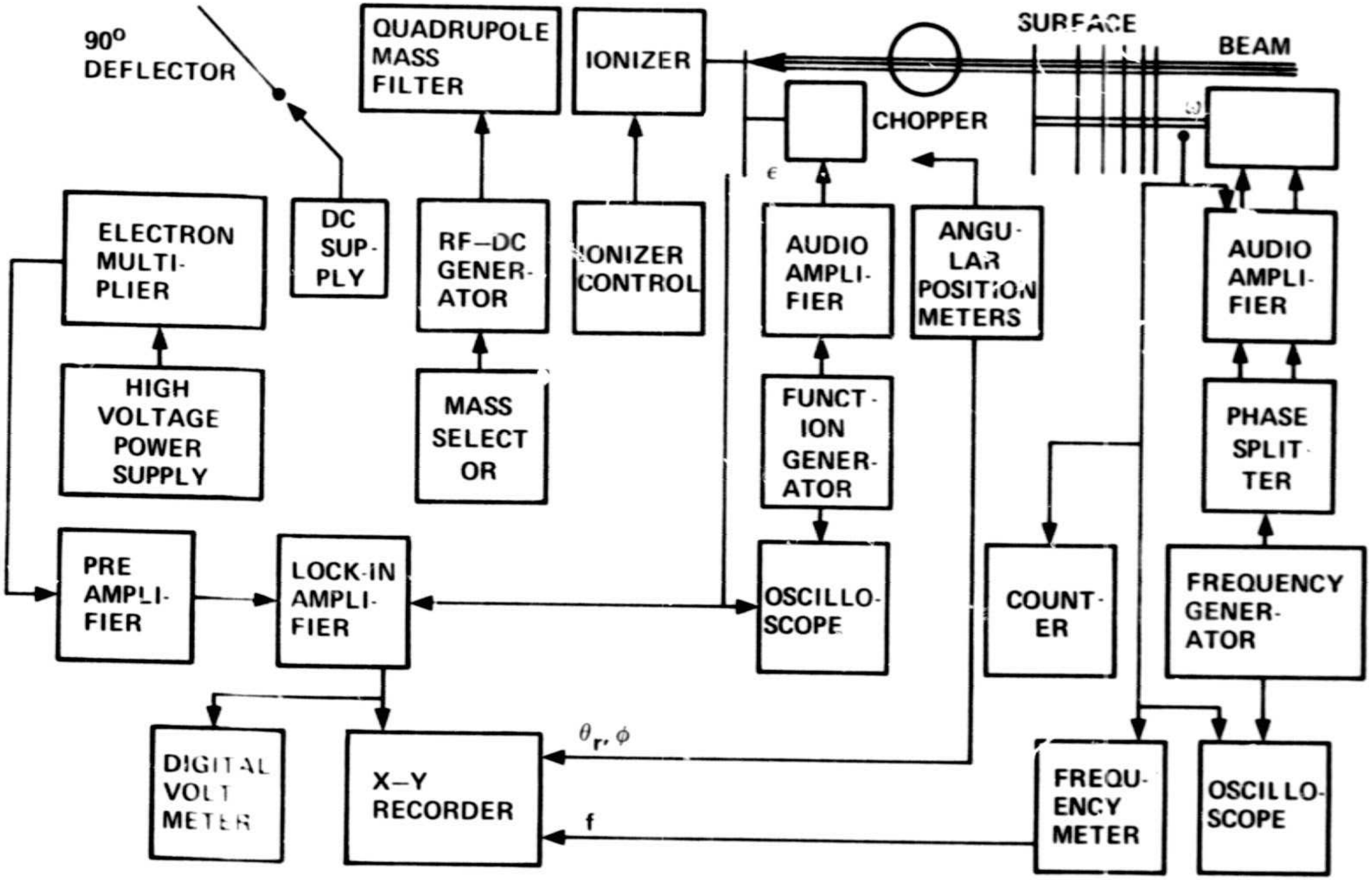

Figure II-3. Block Diagram of the Electronic System of the Mass Spectrometer and the Multi-Disk Velocity Selector.

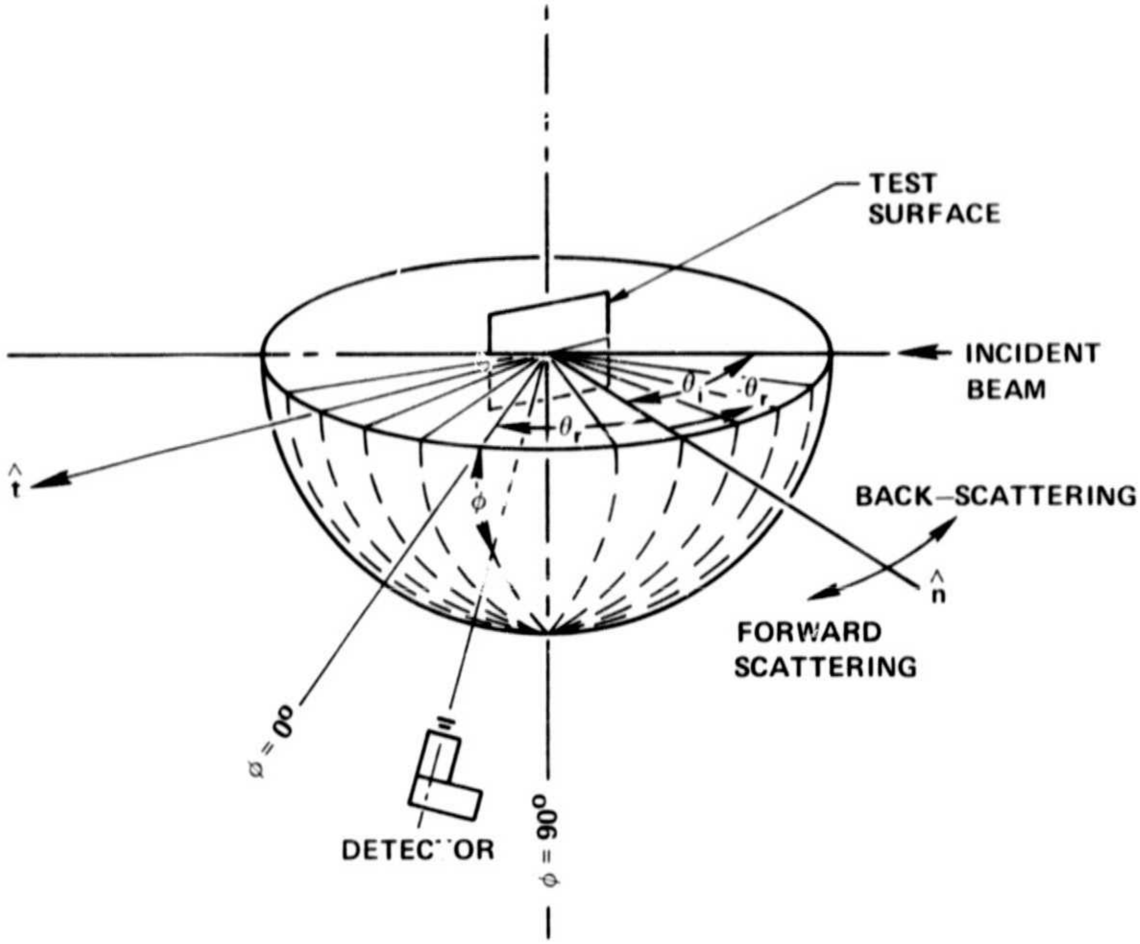

Figure II-4. Schematic Diagram of the Scattering System.

by a multi-disk velocity filter before and after each set of scattering measurements for a given incidence angle. The arc light from the arc-heated supersonic beam source was used for in situ determination of the incidence angle.

CHAPTER III

RESULTS AND DISCUSSIONS

Spatial distributions of a satellite-speed (7000 m/sec) helium beam reflected from four different satellite surfaces (cleaned 6061-T6 aluminum plate, anodized aluminum foil, white paint and quartz surfaces) for six different incidence angles (0°, 15°, 30°, 45°, 60° and 75° from the surface normal) are shown in Figures III-1 to III-24. The center of the polar diagram corresponds to the point of impingement. The incident beam impinges on the test surface (which coincides with the surface of the page) from the bottom of the diagram with the given incidence angle measured from the surface normal. The dashed lines at constant value of θ_r indicate detector paths (i.e. from $\phi = 0°$ to $\phi = 90°$). The upper ($\theta_r > 0°$) and lower ($\theta_r < 0°$) halves of the diagram represent the forward-scattering and backward-scattering regions respectively. The scale of the signal amplitude is arbitrary but self-consistent for each plot. The overall decrease of the signal amplitude in the case of large incidence angle (e.g., $\theta_i \geqq 60°$) is due probably to the fact that a portion of the incident beam (with finite width) misses the target (also with finite width) at glancing incidence angles. Fortunately, this discrepancy will not alter the conclusions and the value of the present results.

As indicated by these plots, the general features of the scattering distributions are similar for all four surfaces tested. The scattering distributions for the normal-incidence case are symmetrical (as expected). As the incidence angle increases toward the surface tangent, the peak of the scattering distribution shifts toward the backward scattering region. This unexpected scattering feature is in contrast with those obtained from well-defined smooth single-crystal surfaces. This large fraction of backscattering

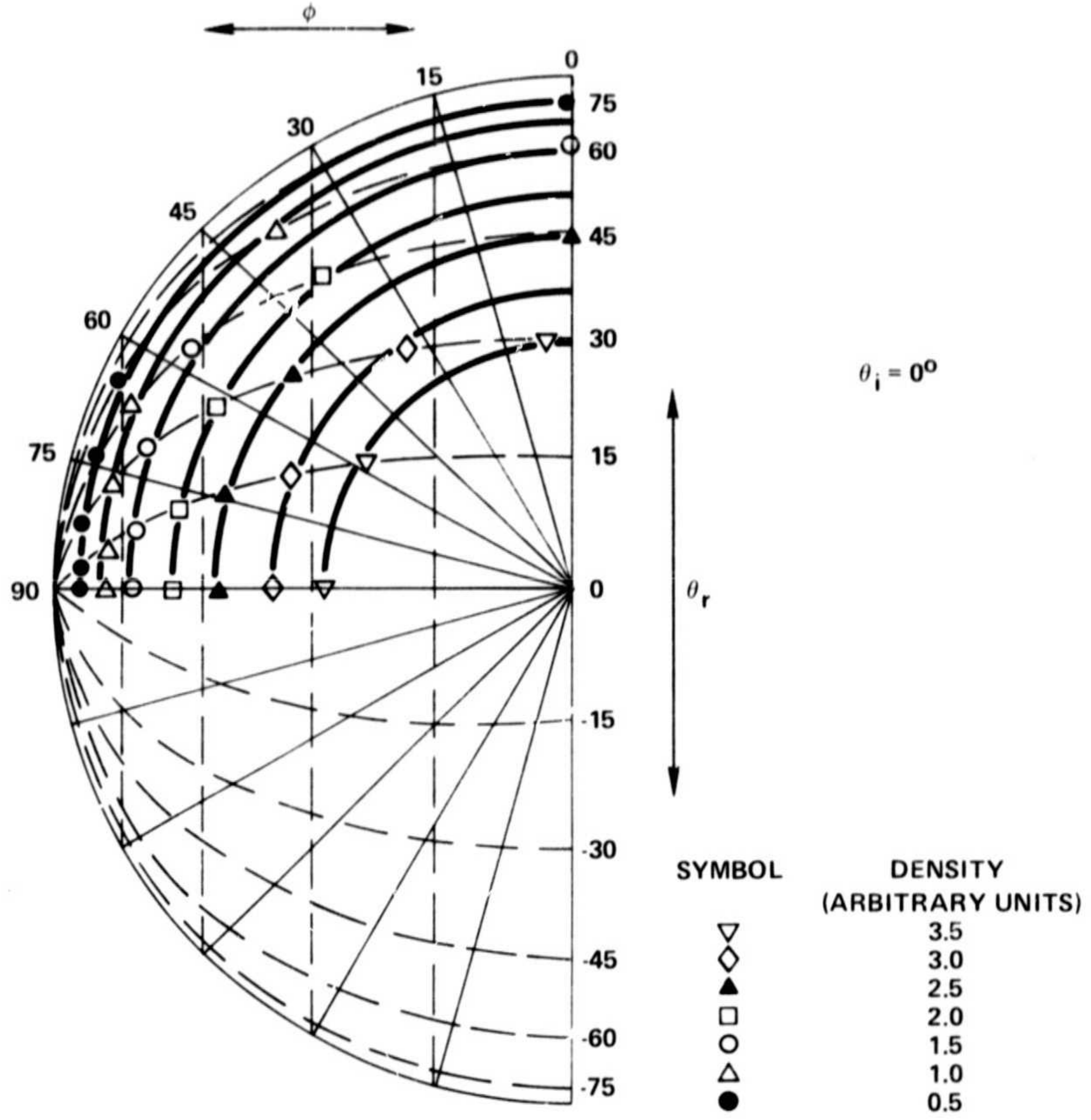

Figure III-1. Polar Plot of Scattered-Beam Density Distribution for 7000 m/sec Helium Beam Scattered from Cleaned 6061-T6 Aluminum Plate at 0° Incidence Angle.

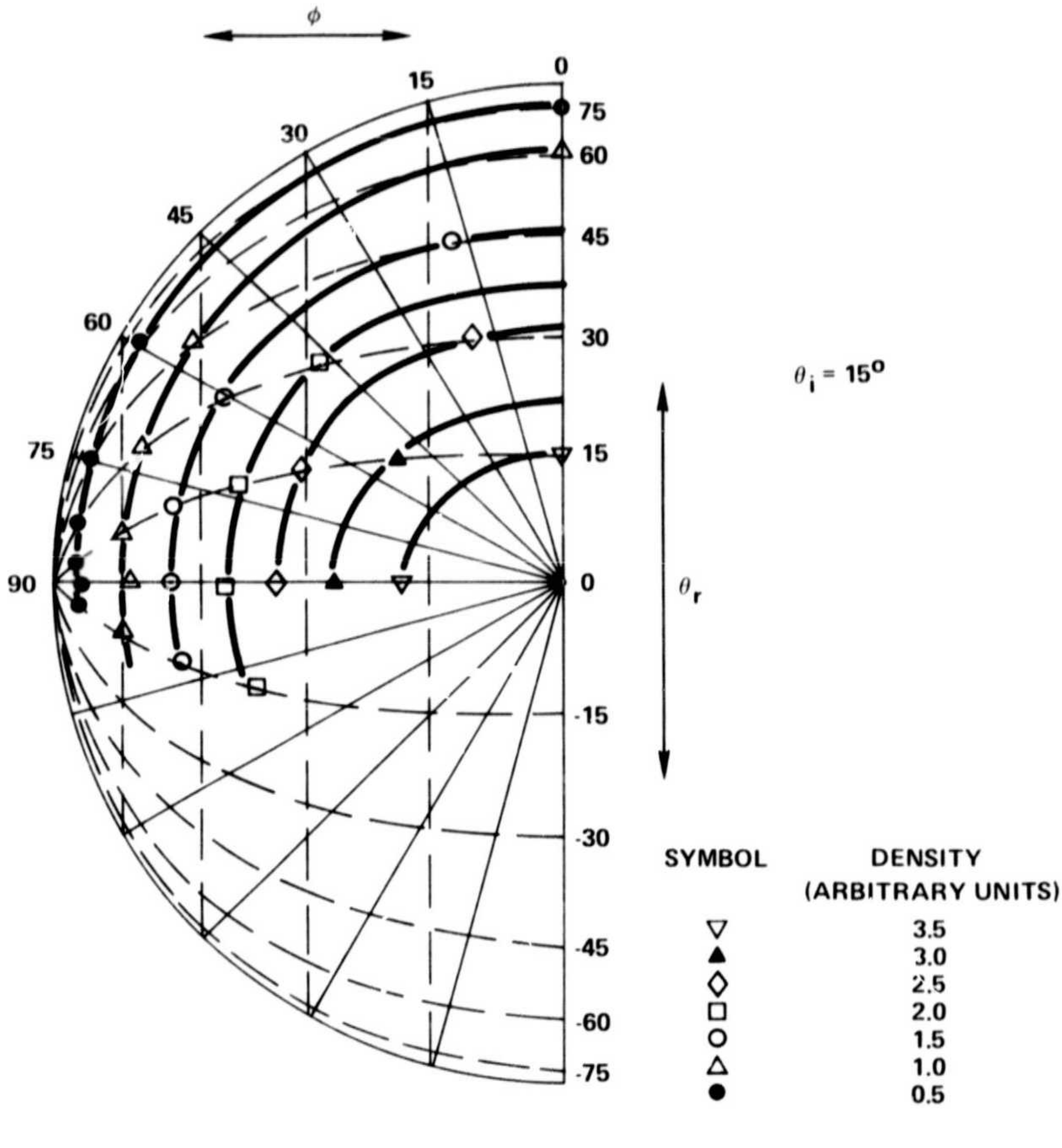

Figure III-2. Polar Plot of Scattered-Beam Density Distribution for 7000 m/sec Helium Beam Scattered from Cleaned 6061-T6 Aluminum Plate at 15° Incidence Angle.

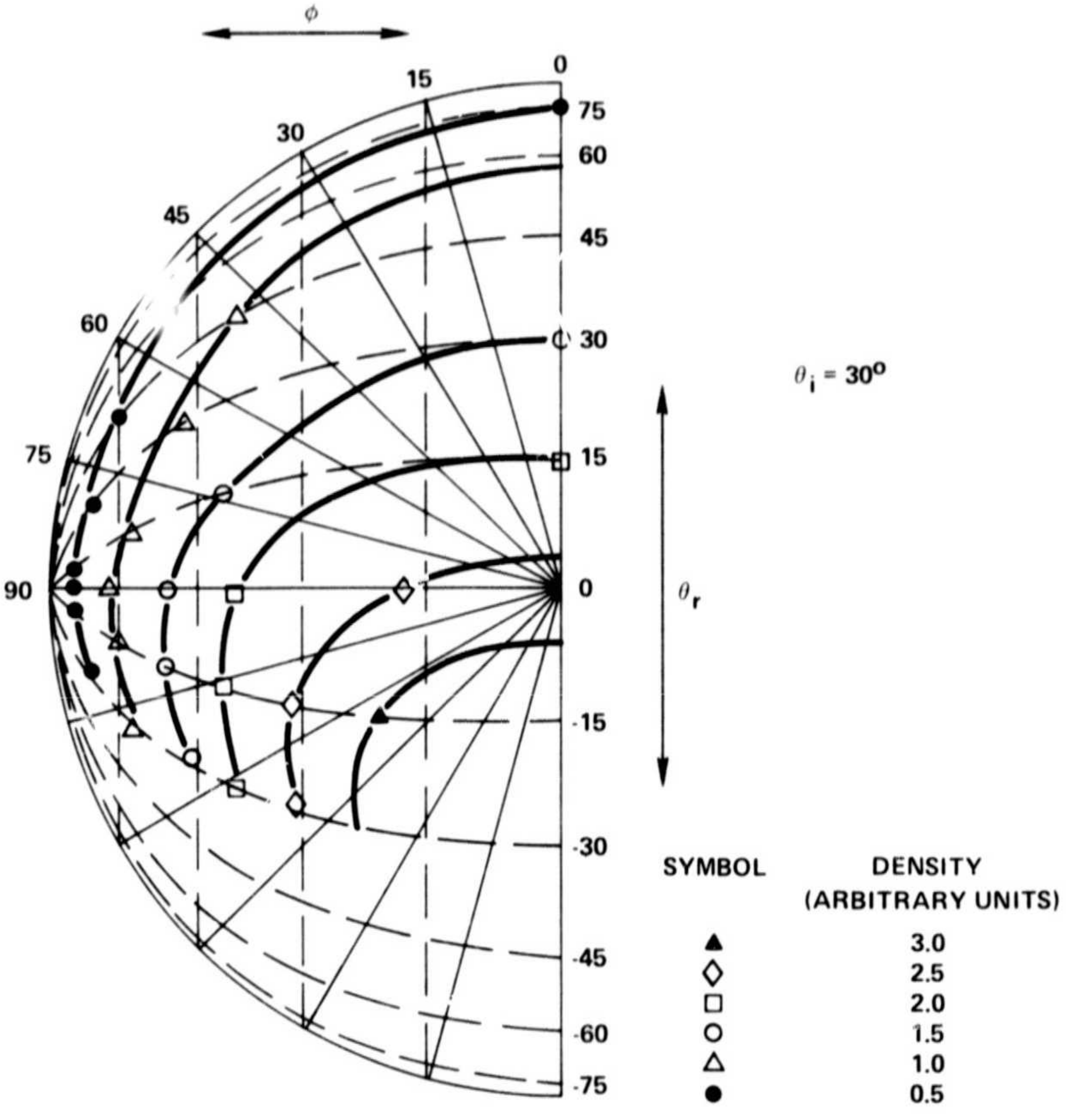

Figure III-3. Polar Plot of Scattered-Beam Density Distribution for 7000 m/sec Helium Beam Scattered from Cleaned 6061-T6 Aluminum Plate at 30° Incidence Angle.

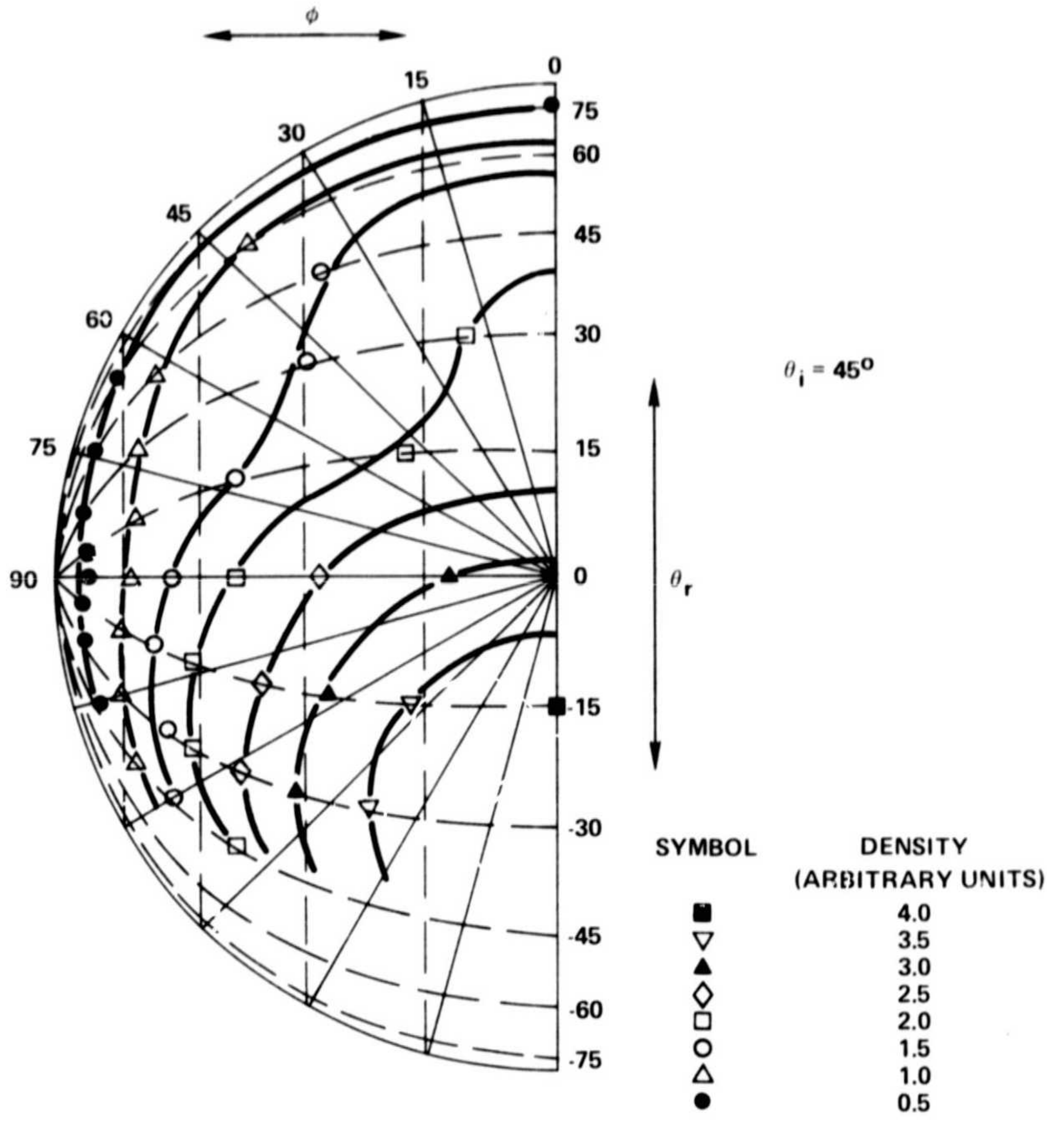

Figure III-4. Polar Plot of Scattered-Beam Density Distribution for 7000 m/sec Helium Beam Scattered from Cleaned 6061-T6 Aluminum Plate at 45° Incidence Angle.

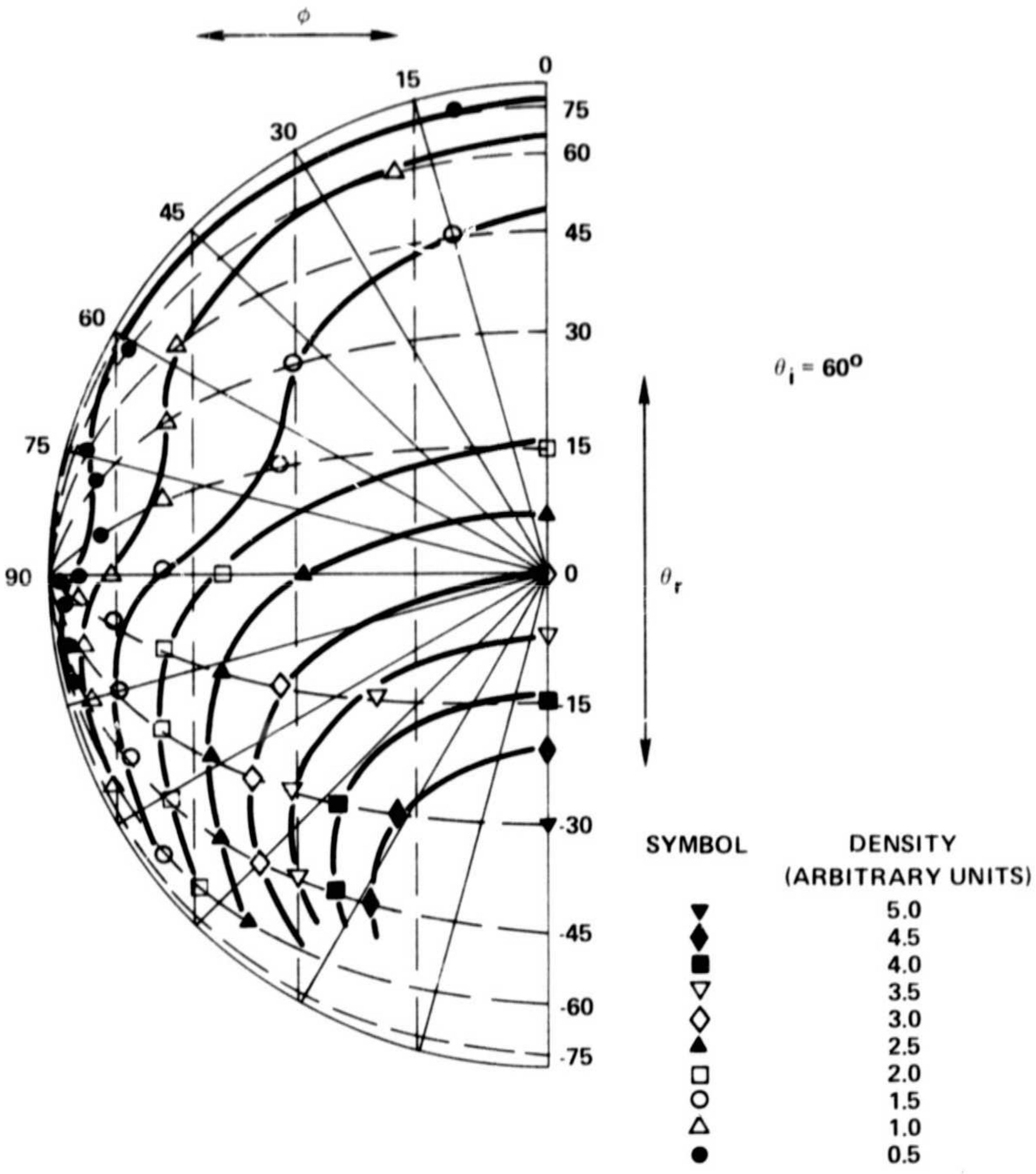

Figure III-5. Polar Plot of Scattered-Beam Density Distribution for 7000 m/sec Helium Beam Scattered from Cleaned 6061-T6 Aluminum Plate at 60° Incidence Angle.

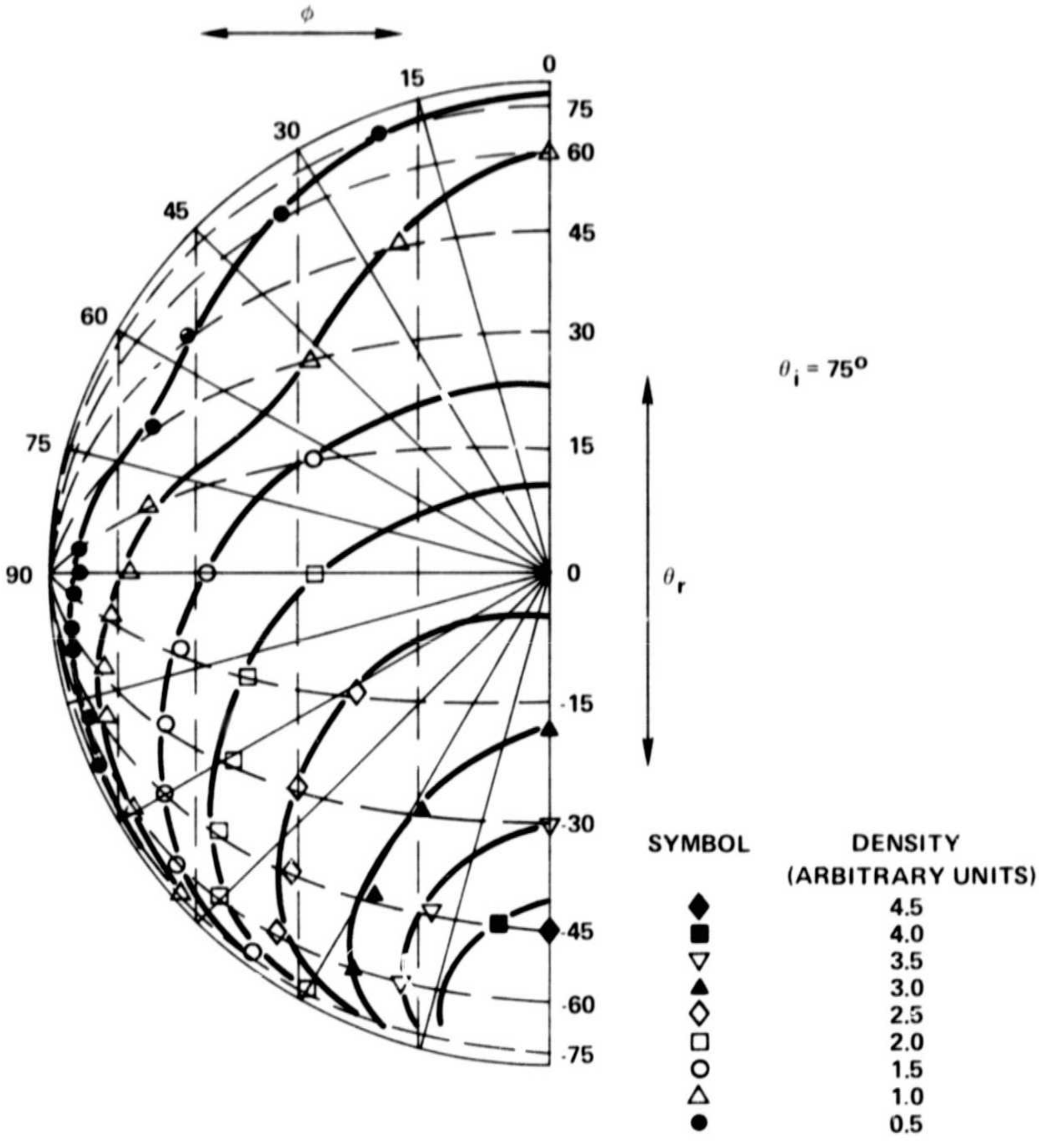

Figure III-6. Polar Plot of Scattered-Beam Density Distribution for 7000 m/sec Helium Beam Scattered from Cleaned 6061-T6 Aluminum Plate at 75° Incidence Angle.

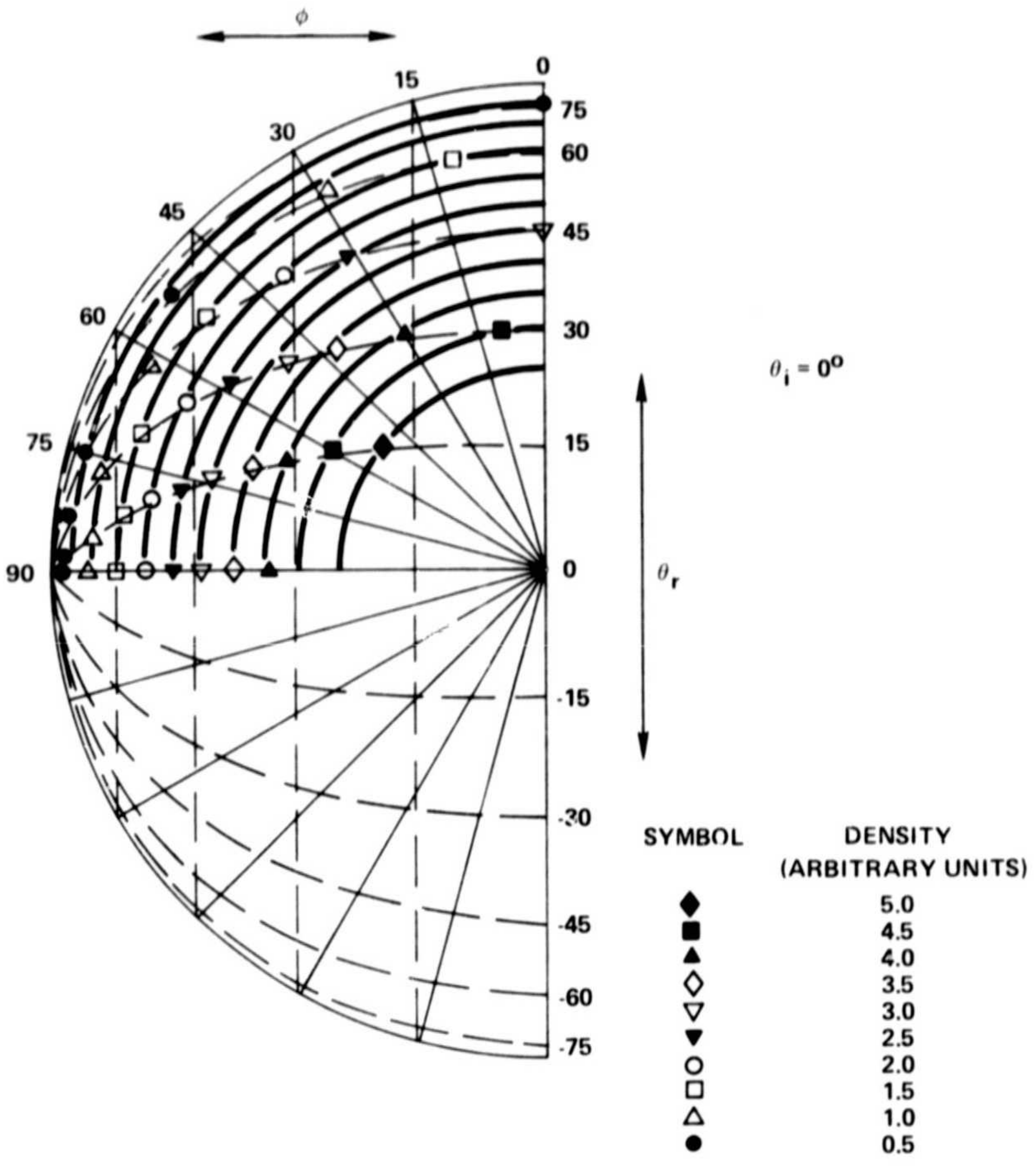

Figure III-7. Polar Plot of Scattered-Beam Density Distribution for 7000 m/sec Helium Beam Scattered from Anodized Aluminum Foil at 0^o incidence Angle.

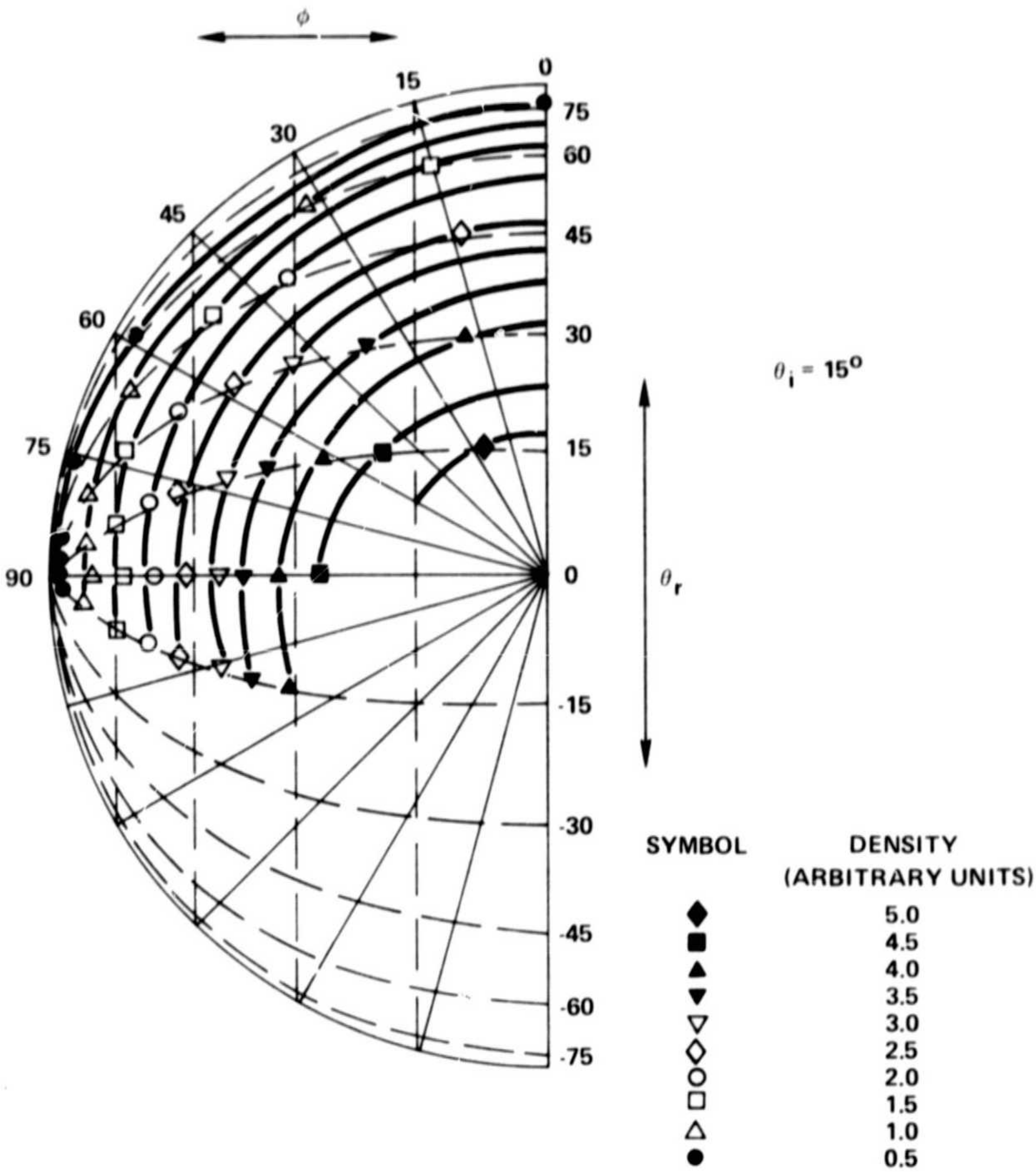

Figure III-8. Polar Plot of Scattered-Beam Density Distribution for 7000 m/sec Helium Beam Scattered from Anodized Aluminum Foil at 15° Incidence Angle.

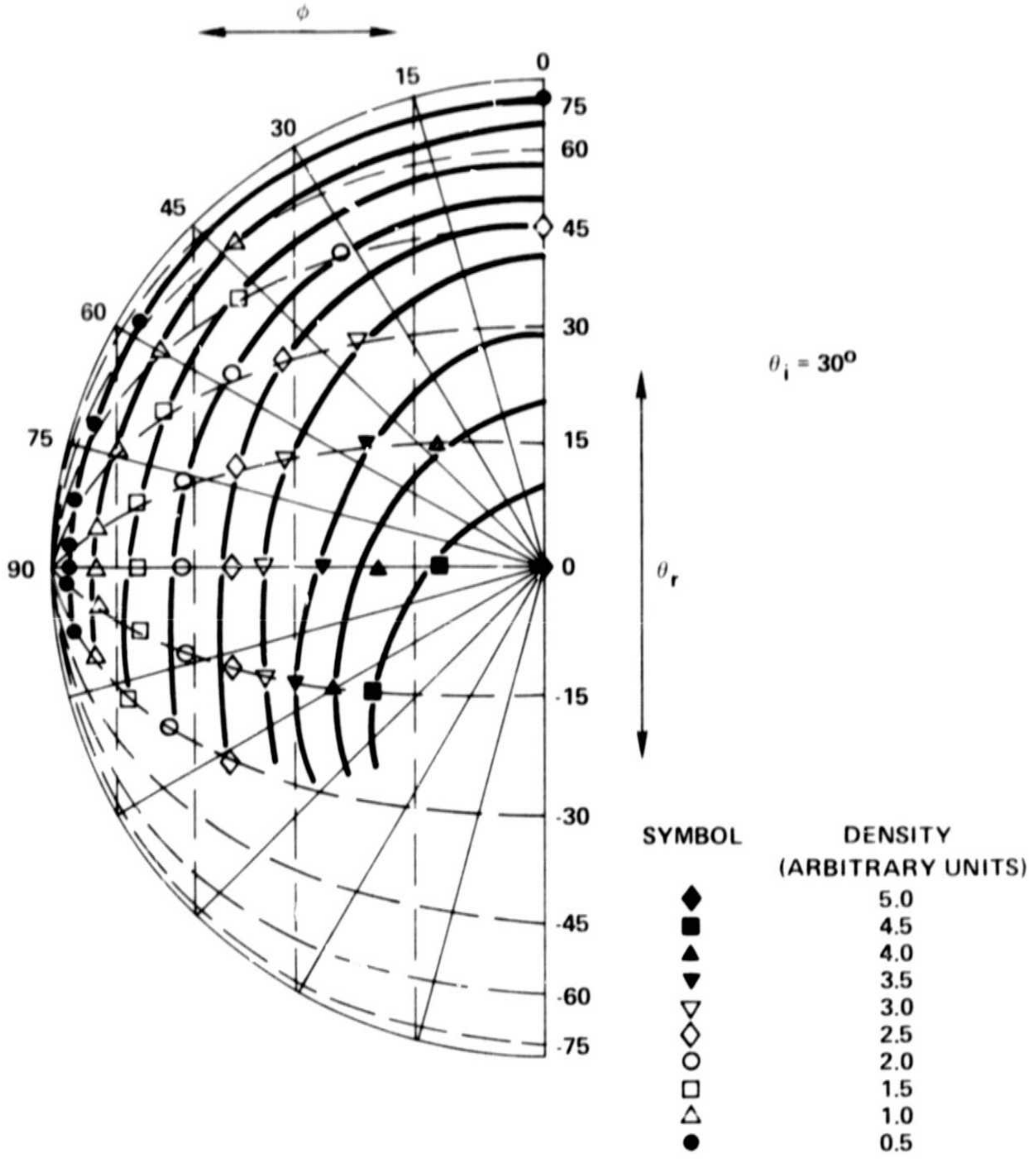

Figure III-9. Polar Plot of Scattered-Beam Density Distribution for 7000 m/sec Helium Beam Scattered from Anodized Aluminum Foil at 30° Incidence Angle.

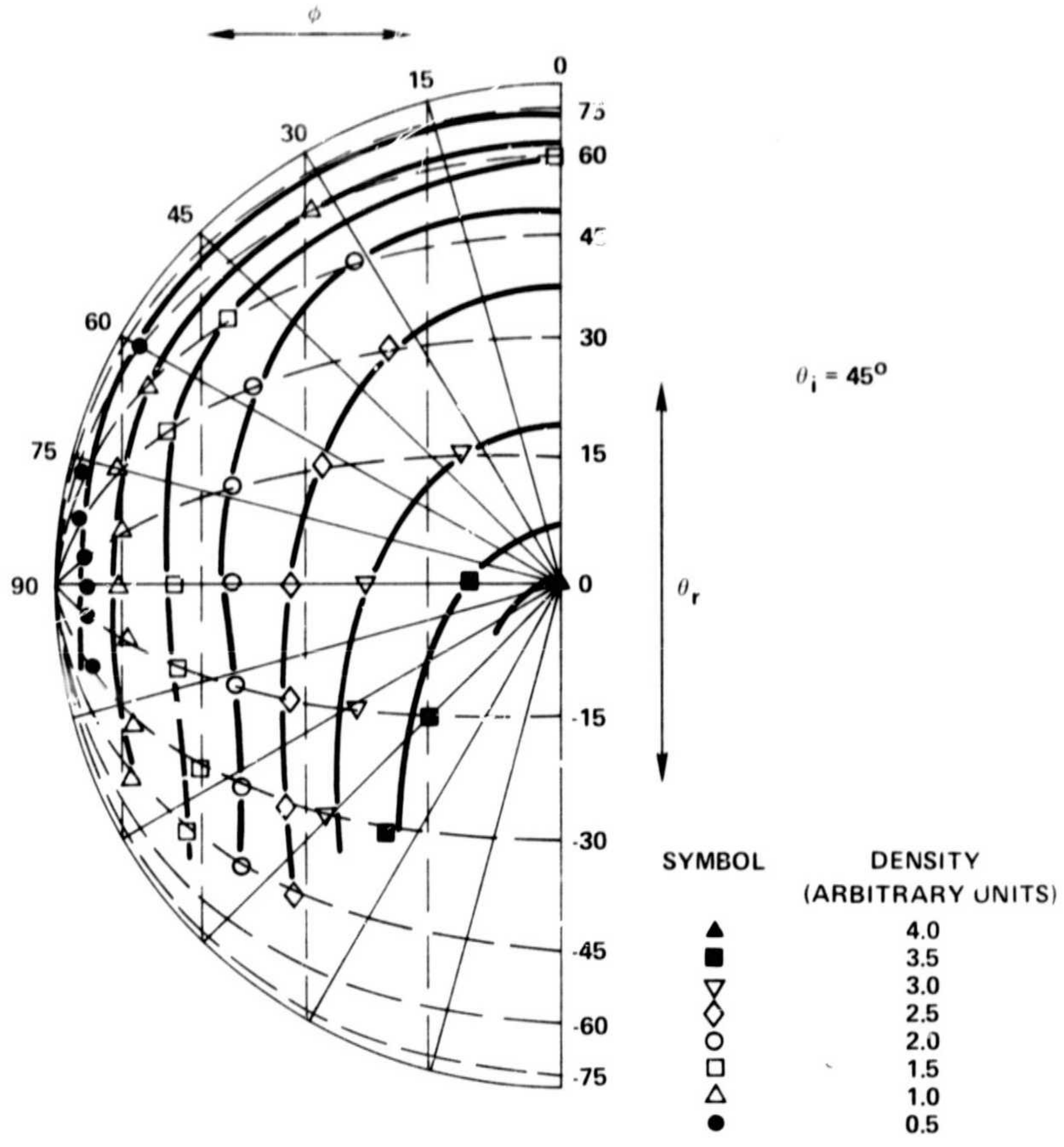

Figure III-10. Polar Plot of Scattered-Beam Density Distribution for 7000 m/sec Helium Beam Scattered from Anodized Aluminum Foil at 45° Incidence Angle.

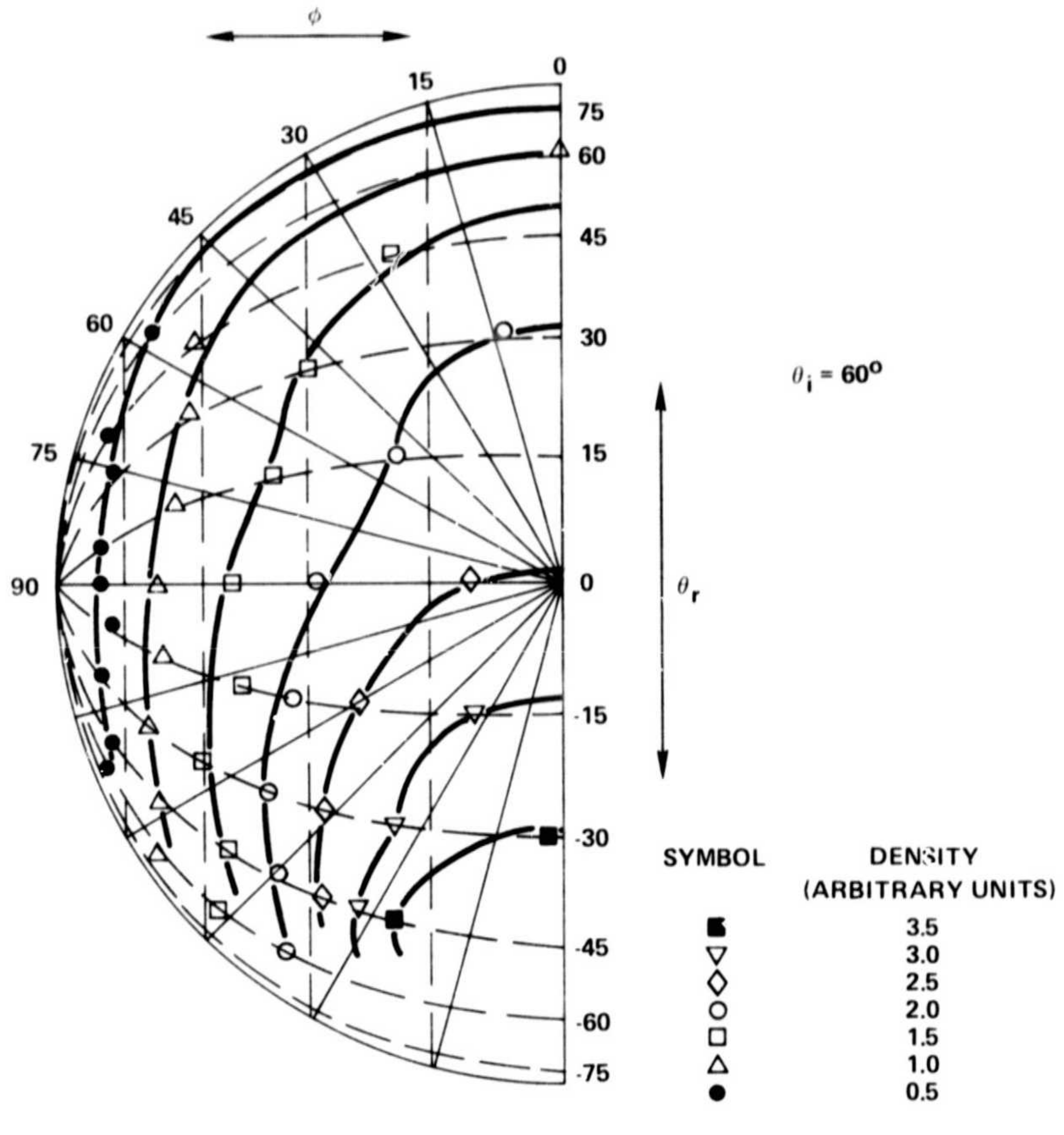

Figure III-11. Polar Plot of Scattered-Beam Density Distribution for 7000 m/sec Helium Beam Scattered from Anodized Aluminum Foil at 60° Incidence Angle.

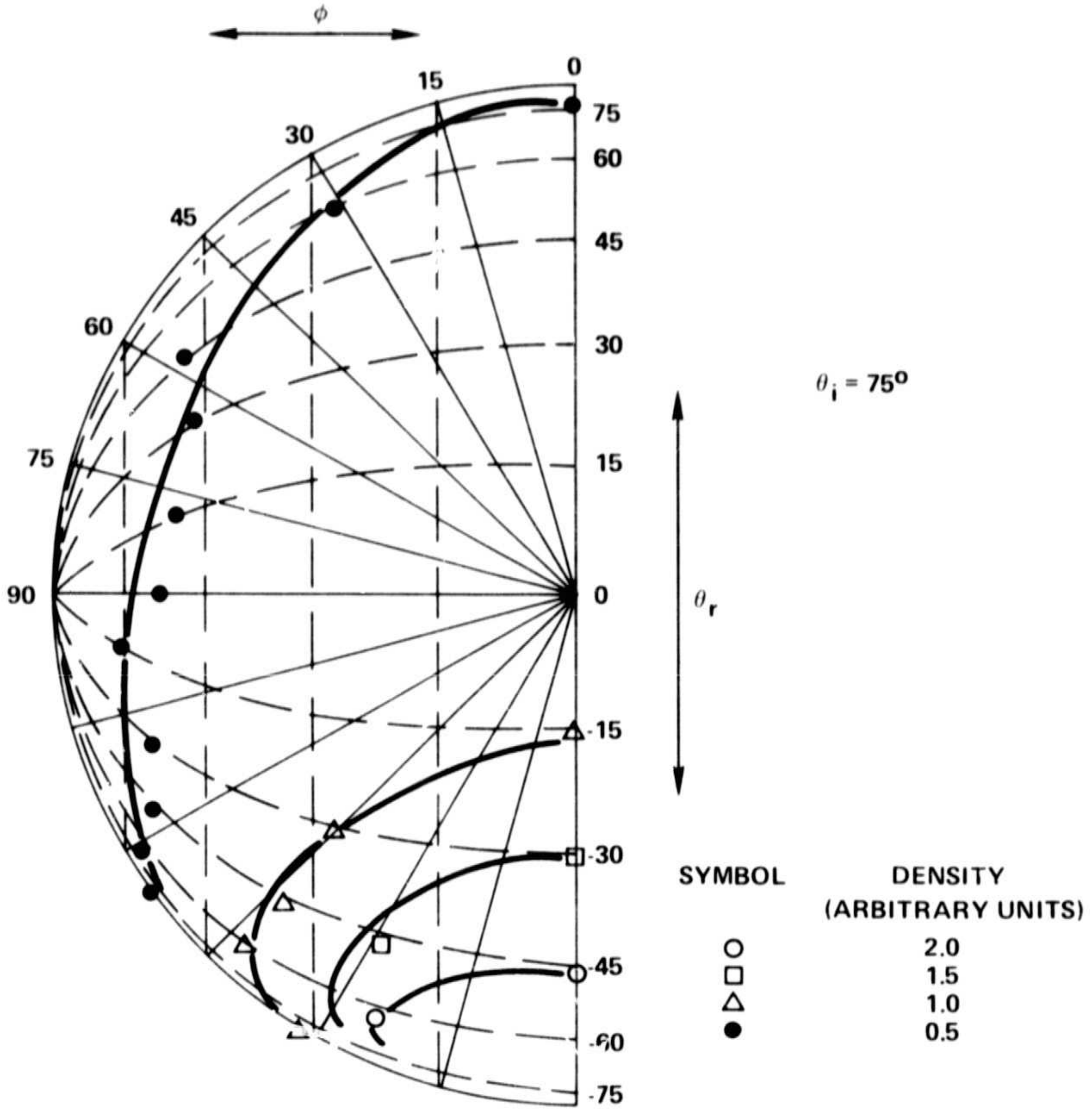

Figure III-12. Polar Plot of Scattered-Beam Density Distribution for 7000 m/sec Helium Beam Scattered from Anodized Aluminum Foil at 75° Incidence Angle.

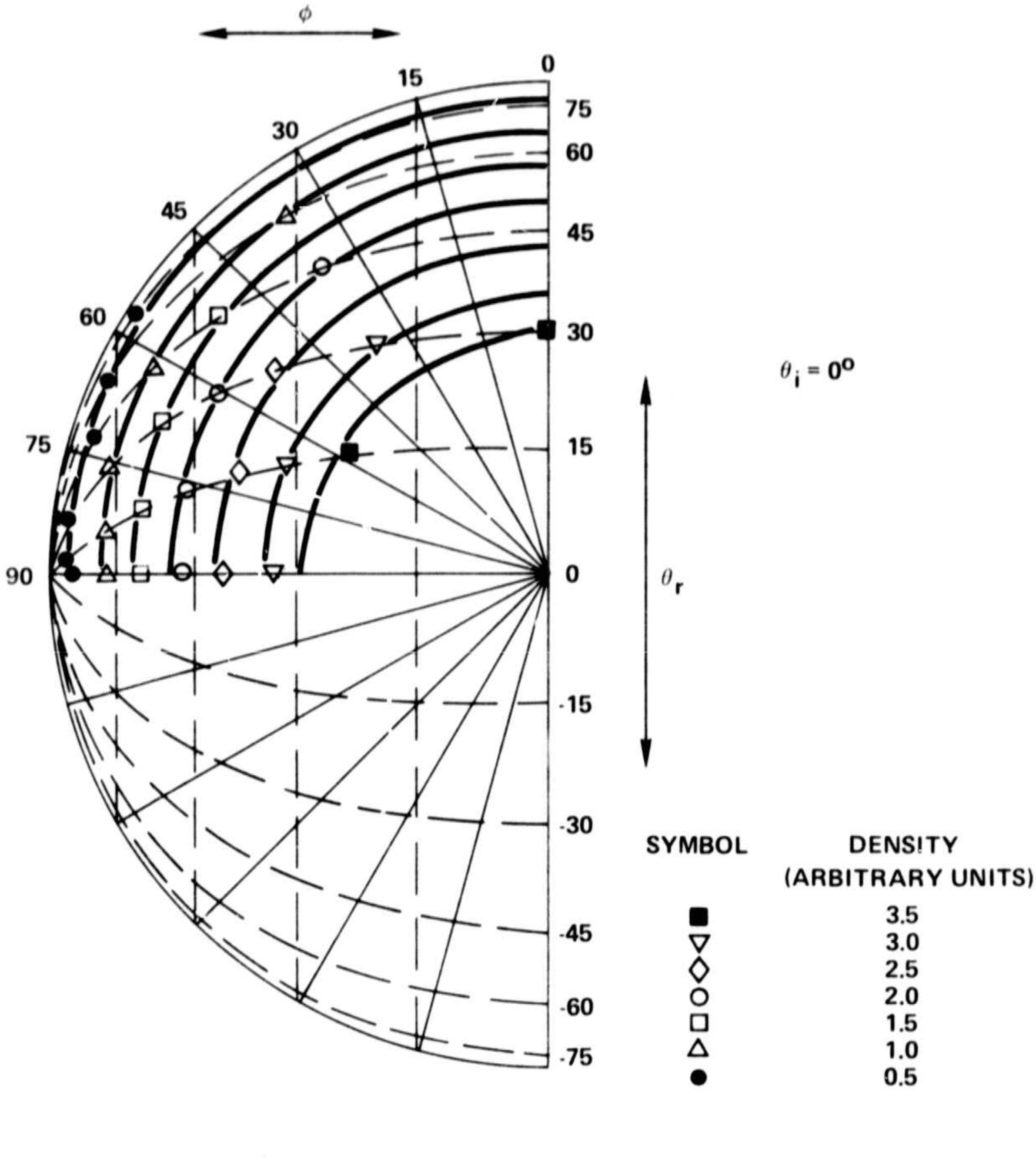

Figure III-13. Polar Plot of Scattered-Beam Density Distribution for 7000 m/sec Helium Beam Scattered from White Paint Surface at 0° Incidence Angle.

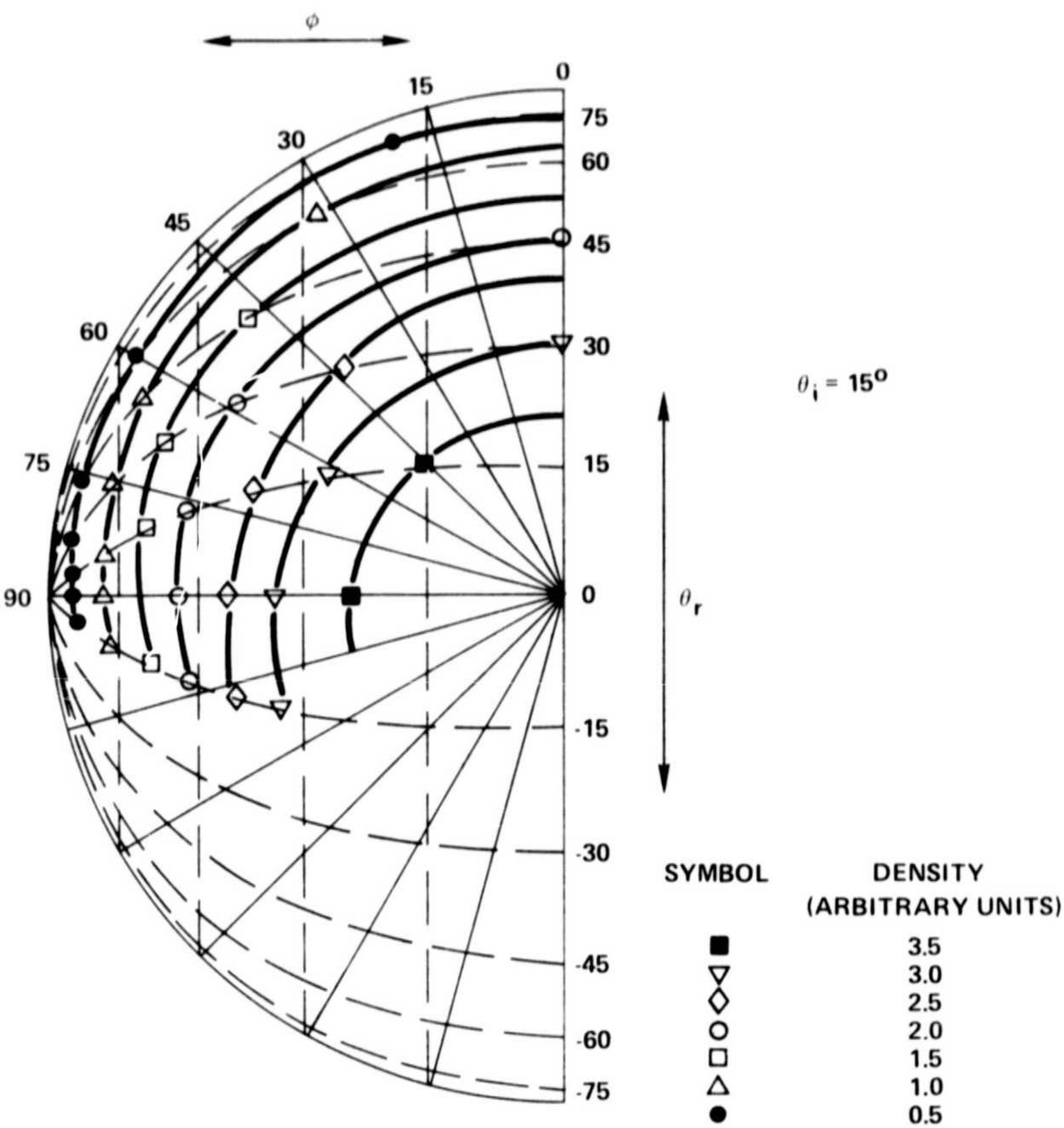

Figure III-14. Polar Plot of Scattered-Beam Density Distribution for 7000 m/sec Helium Beam Scattered from White Paint Surface at 15° Incidence Angle.

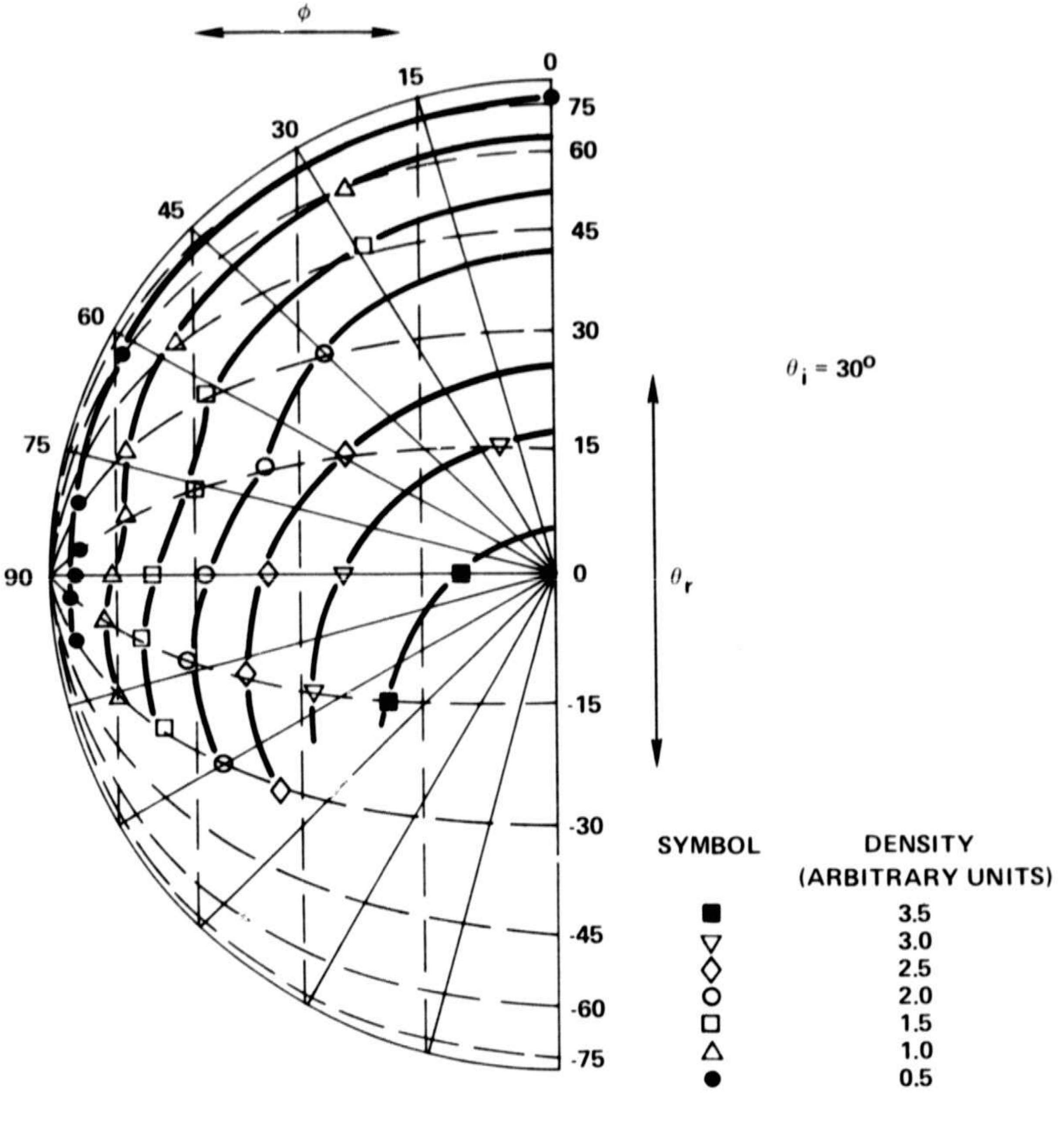

Figure III-15. Polar Plot of Scattered-Beam Density Distribution for 7000 m/sec Helium Beam Scattered from White Paint Surface at 30° Incidence Angle

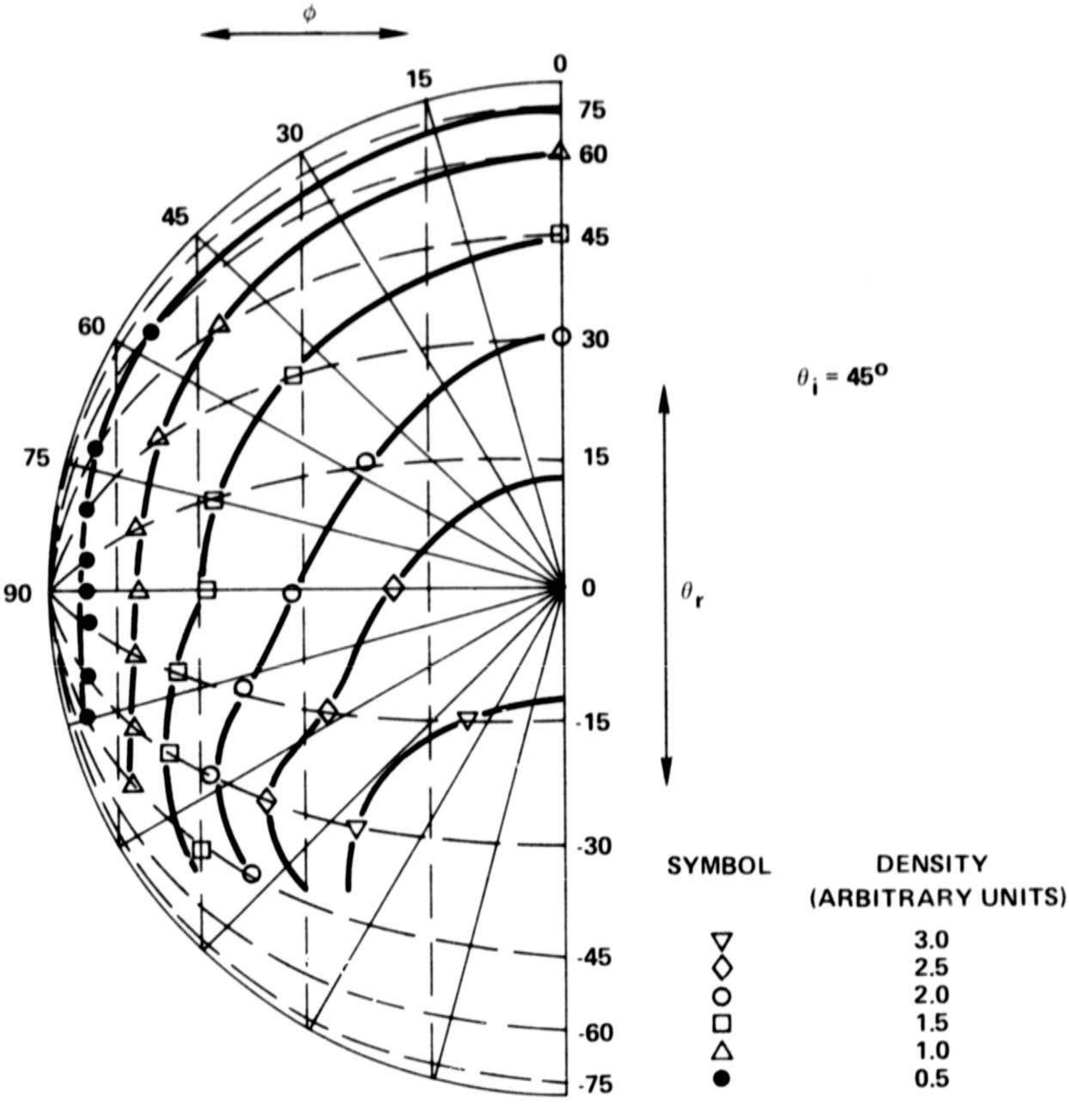

Figure III-16. Polar Plot of Scattered-Beam Density Distribution for 7000 m/sec Helium Beam Scattered from White Paint Surface at 45° Incidence Angle.

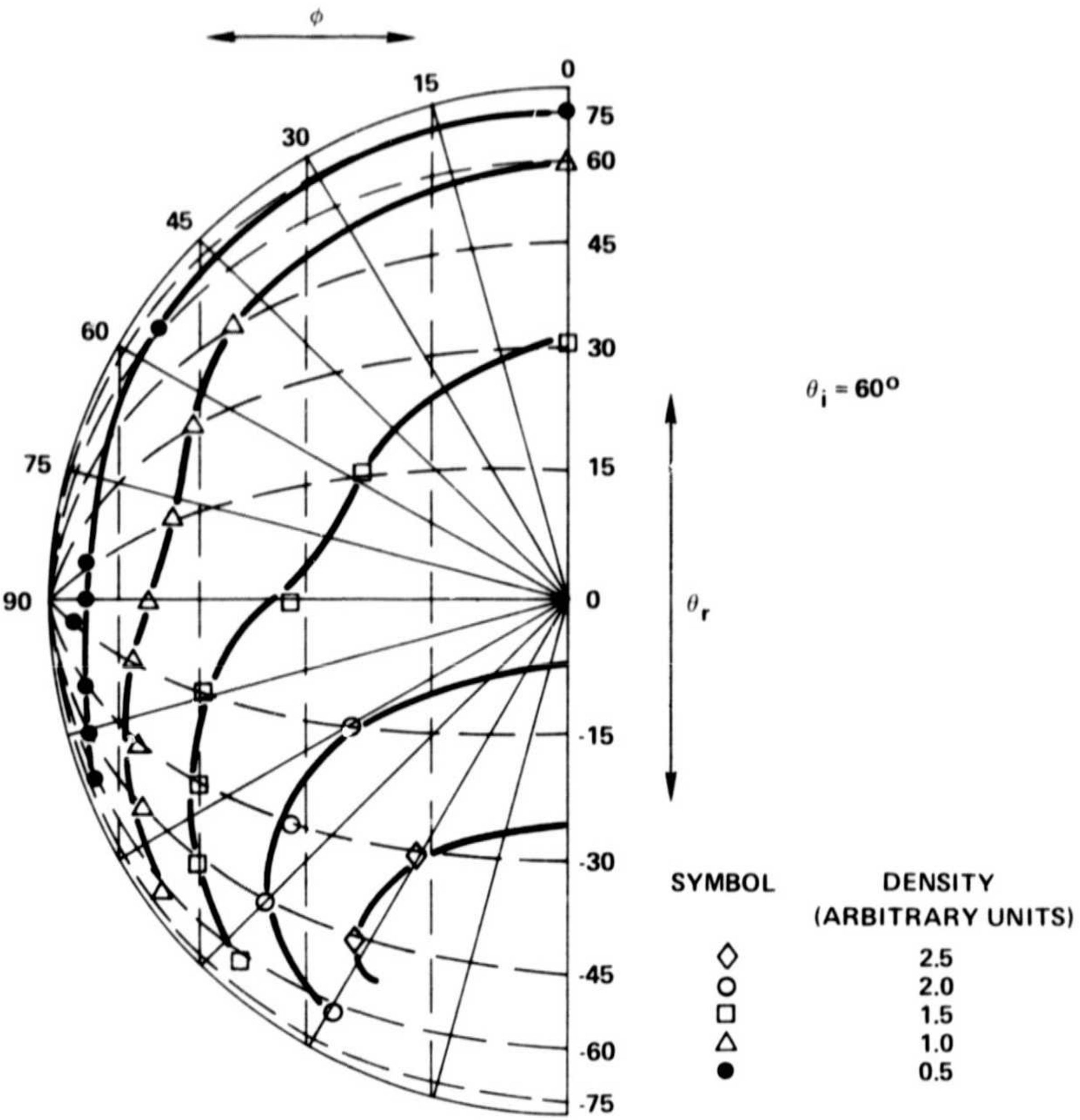

Figure III-17. Polar Plot of Scattered-Beam Density Distribution for 7000 m/sec Helium Beam Scattered from White Paint Surface at 60° Incidence Angle.

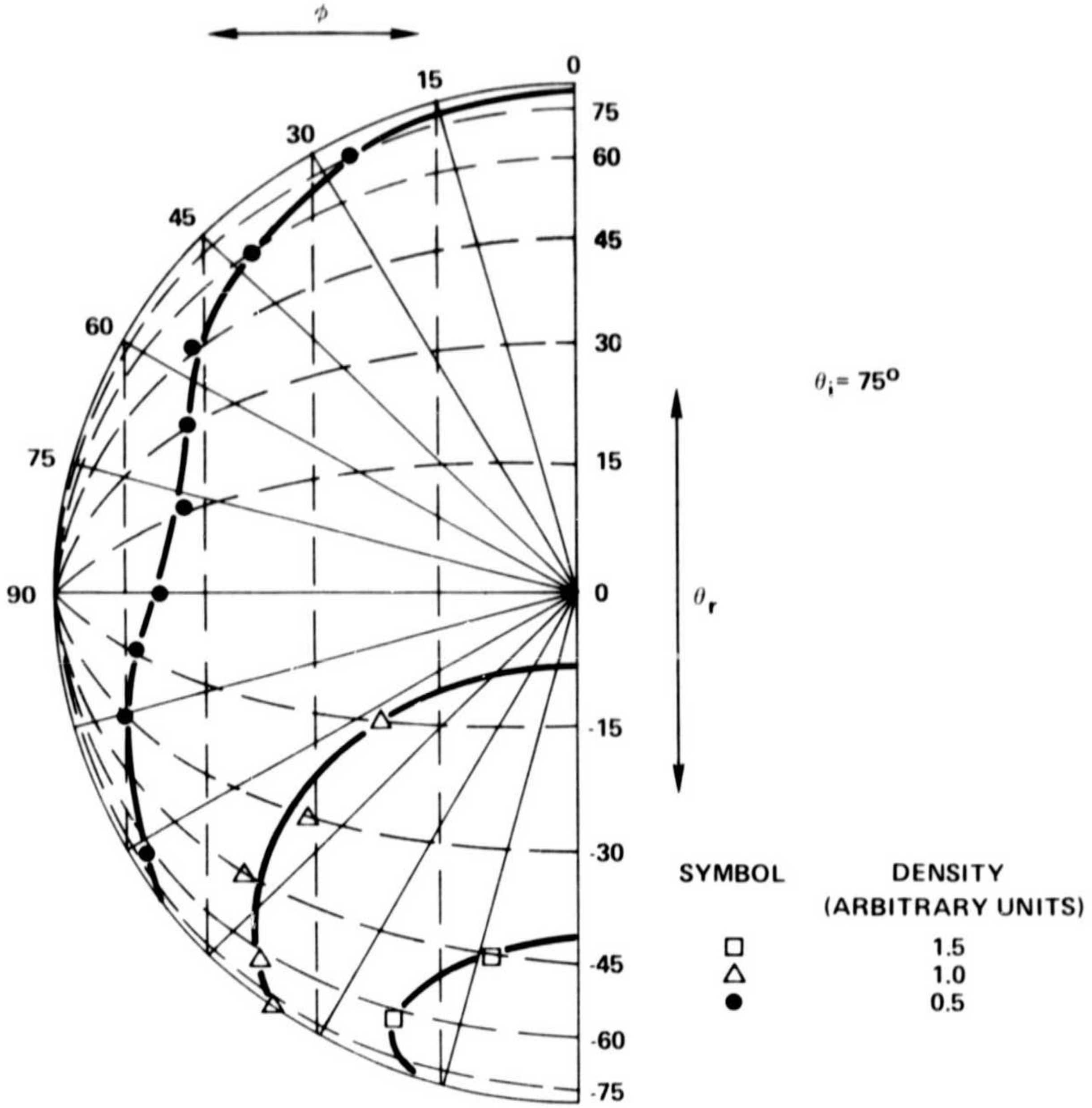

Figure III-18. Polar Plot of Scattered-Beam Density Distribution for 7000 m/sec Helium Beam Scattered from White Paint Surface at 75° Incidence Angle.

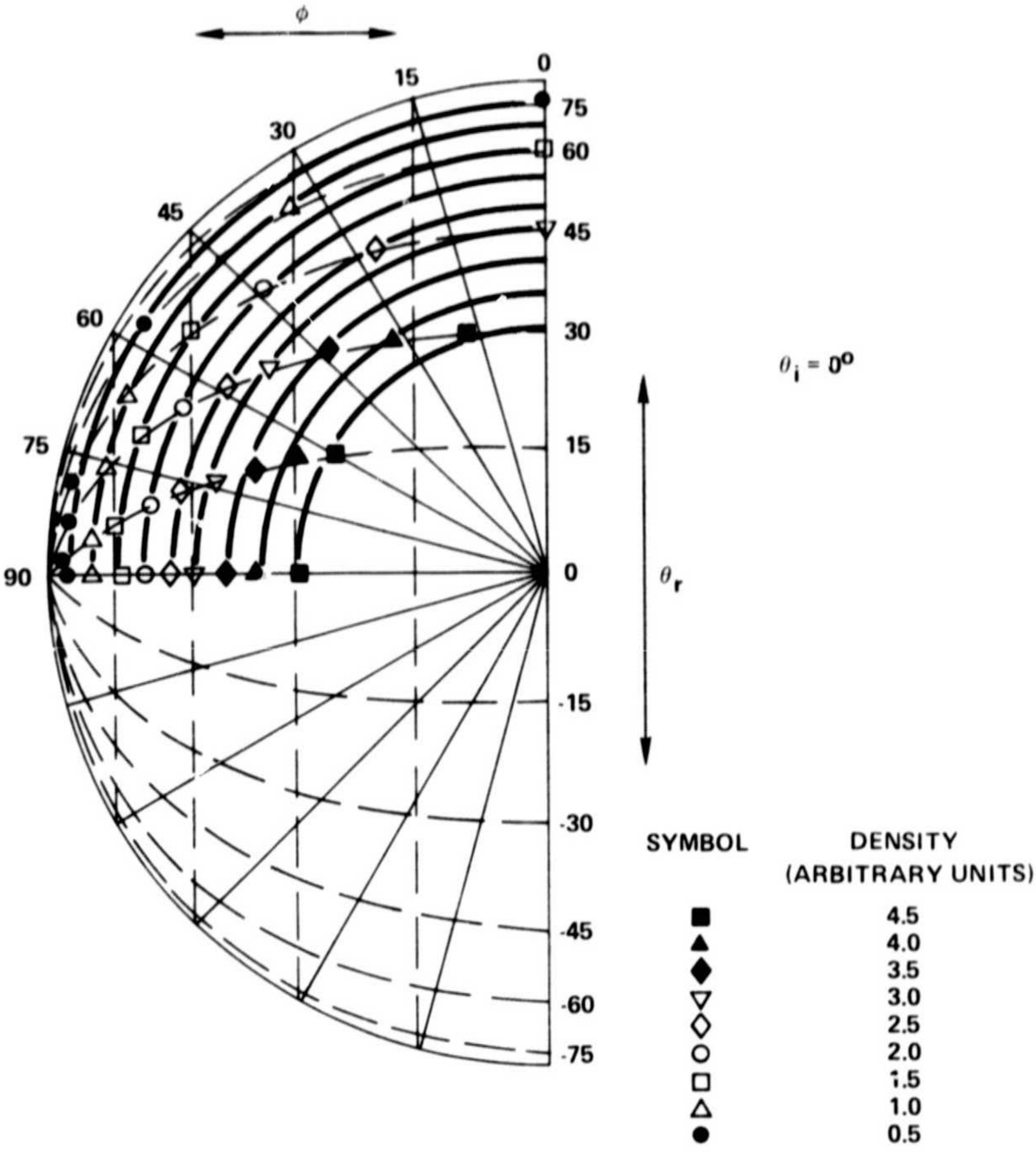

Figure III-19. Polar Plot of Scattered-Beam Density Distribution for 7000 m/sec Helium Beam Scattered from Quartz Surface at 0° Incidence Angle.

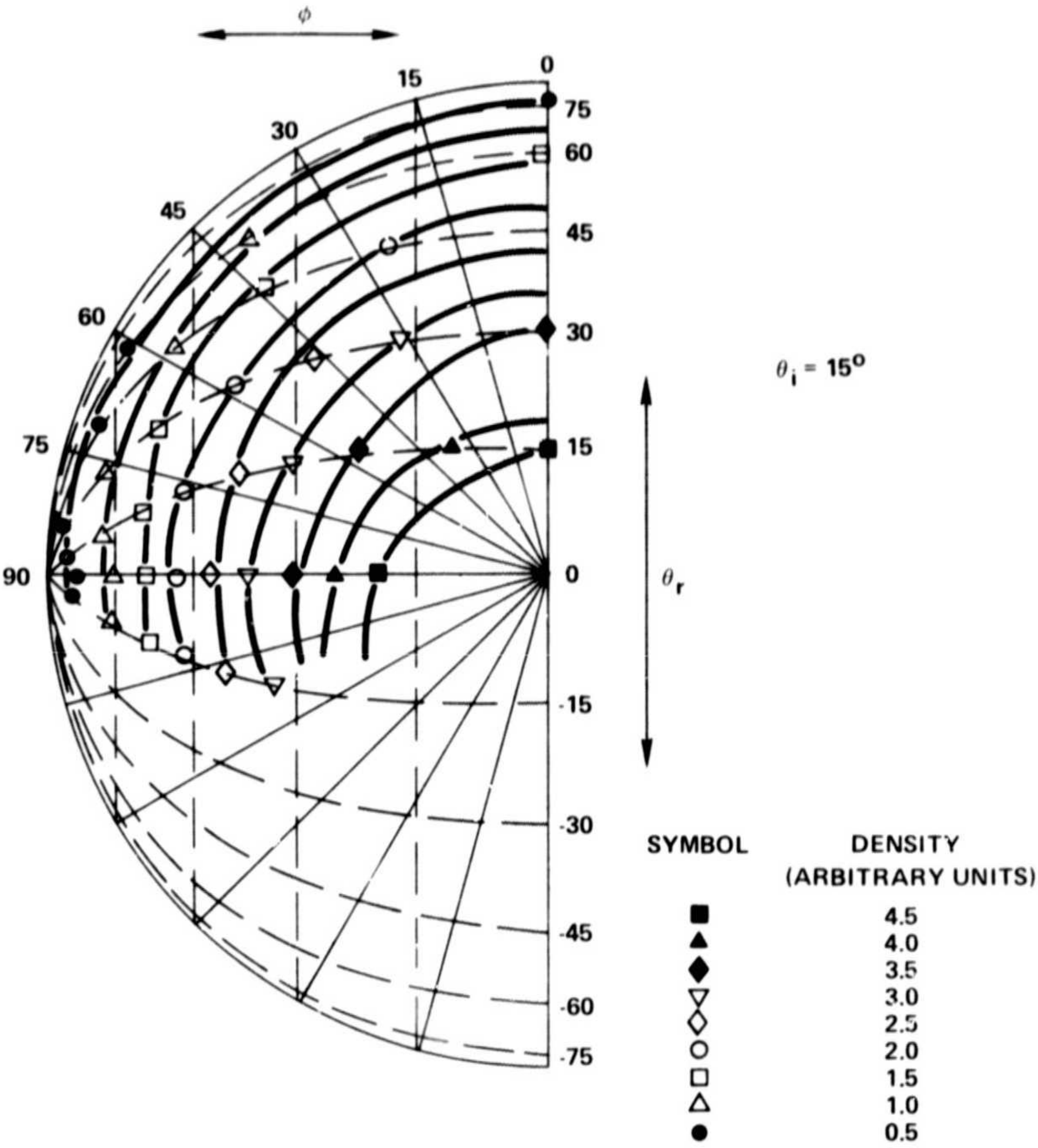

Figure III-20. Polar Plot of Scattered-Beam Density Distribution for 7000 m/sec Helium Beam Scattered from Quartz Surface at 15° Incidence Angle.

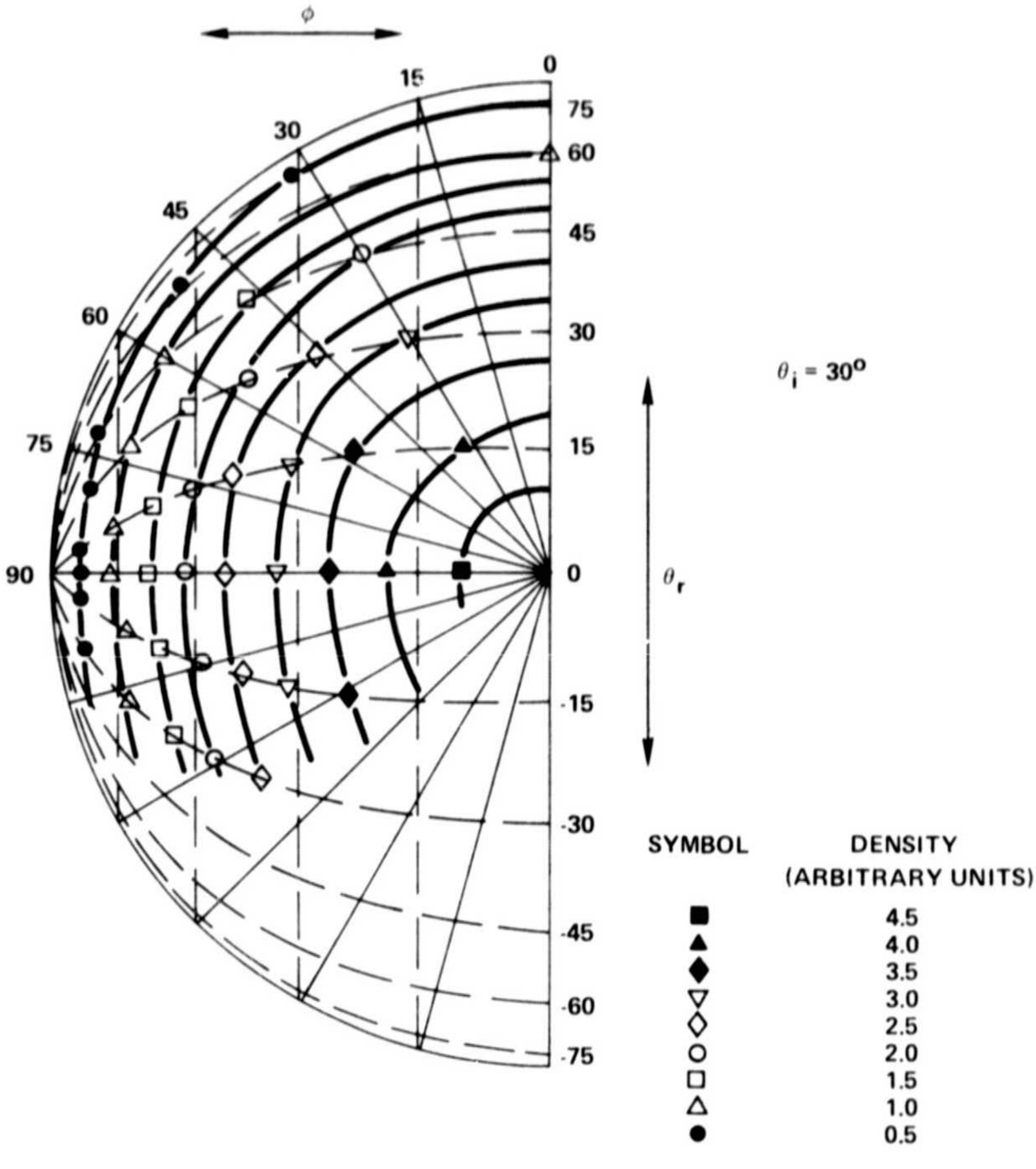

Figure III-21. Polar Plot of Scattered-Beam Density Distribution for 7000 m/sec Helium Beam Scattered from Quartz Surface at 30° Incidence Angle.

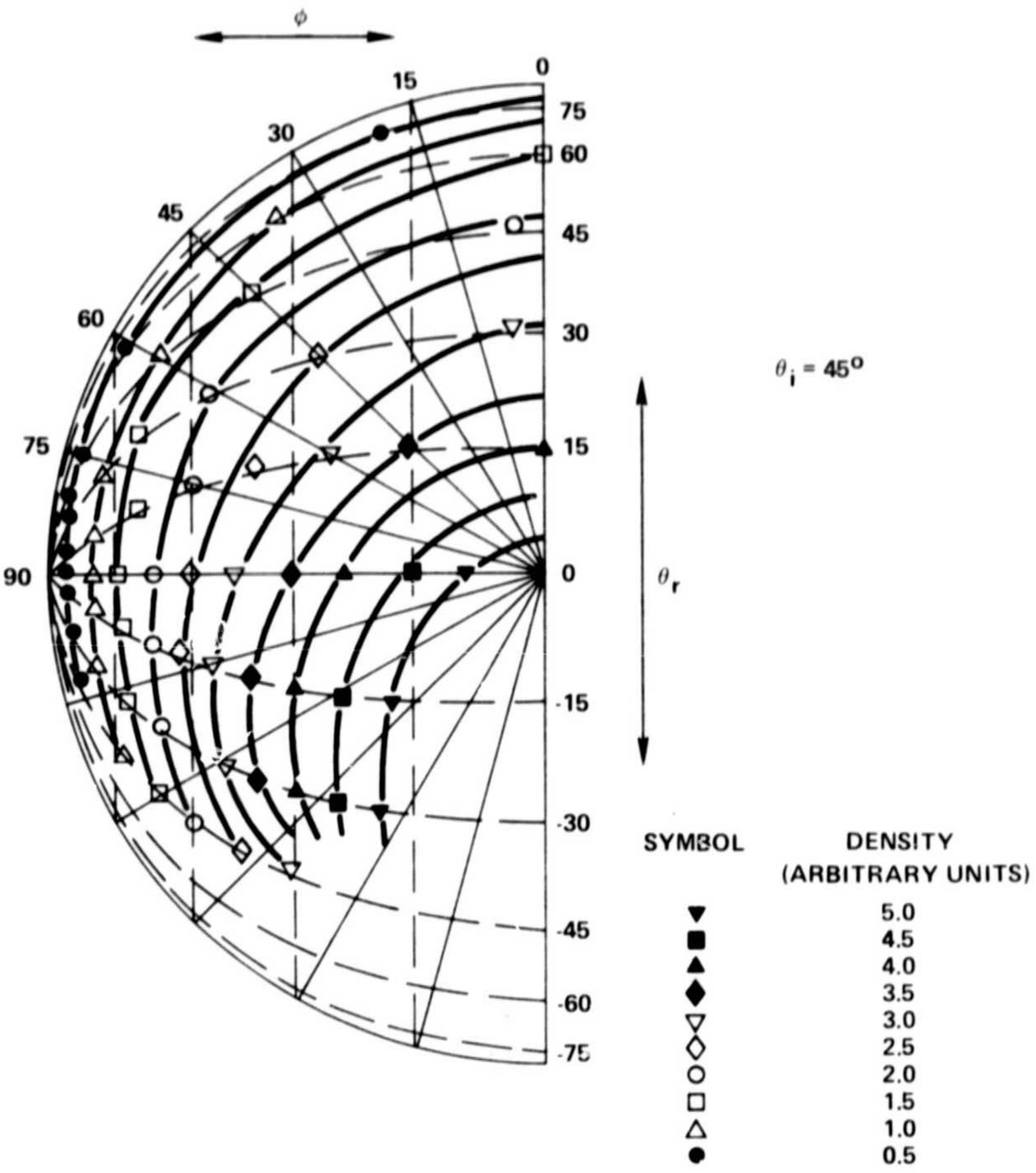

Figure III-22. Polar Plot of Scattered-Beam Density Distribution for 7000 m/sec Helium Beam Scattered from Quartz Surface at 45° Incidence Angle.

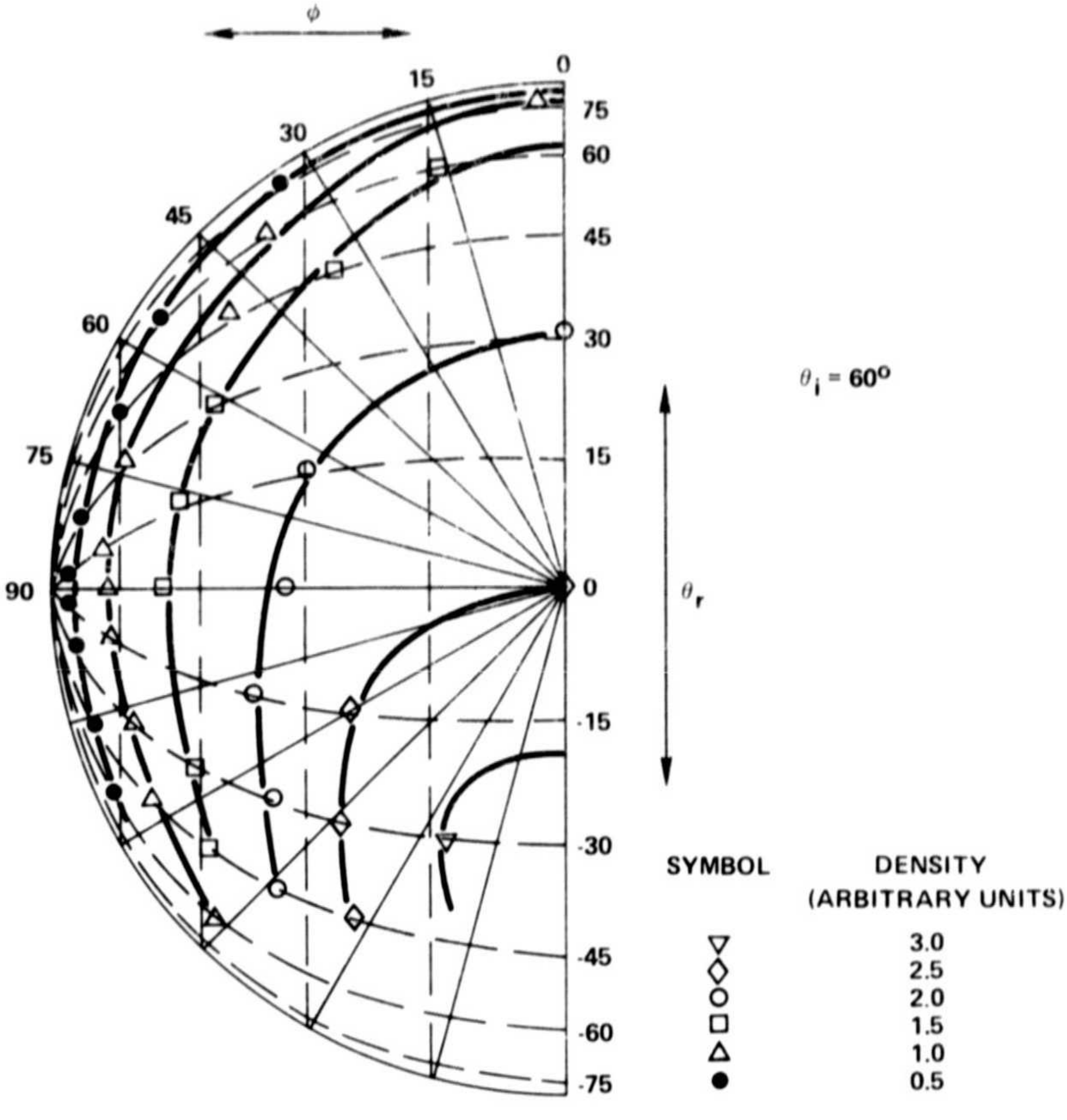

Figure III-23. Polar Plot of Scattered-Beam Density Distribution for 7000 m/sec Helium Beam Scattered from Quartz Surface at 60° Incidence Angle.

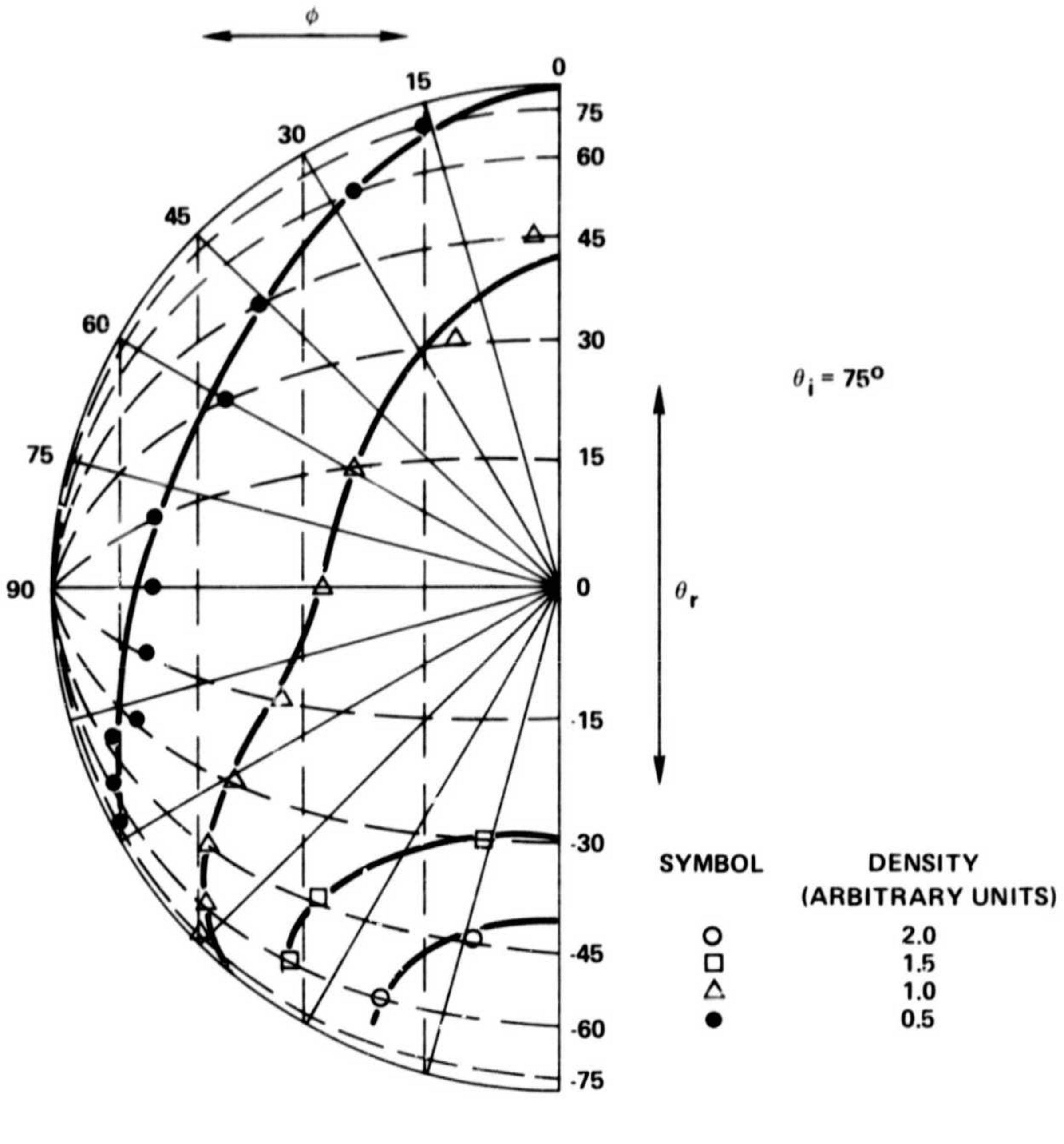

Figure III-24. Polar Plot of Scattered-Beam Density Distribution for 7000 m/sec Helium Beam Scattered from Quartz Surface at 75° Incidence Angle.

could be due to the gross surface roughness of these satellite surfaces. Furthermore, if a large fraction of incoming helium atoms are scattered back with momentum in the direction opposite to the incident-beam momentum, then the drag for these satellite surfaces may be relatively high.

When the spatial-distribution measurements reported here are combined with the energy distribution measurements (to be presented as Part II of this study in a future report), then the overall momentum accommodation coefficient (therefore the drag coefficient) for satellite-speed helium atoms interacting with satellite surfaces may be evaluated.

REFERENCES

1. Calia, V. S., and R. A. Oman, "Scattering Cross-Section Measurements for Epithermal Ar on Ag(111) Surfaces," J. Chem. Phys. 52:6184-6188, 1970.

2. Romney, M. J., and J. B. Anderson, "Scattering of 0.05-5 eV Argon from the (111) Plane of Silver," J. Chem. Phys. 51:2490-2496, 1969.

3. Miller, D. R., and R. B. Subbarao, "Scattering of 0.06-2.5 eV Neon and Argon Atoms from a Silver (111) Crystal," J. Chem. Phys. 52: 425-431, 1970.

4. Hays, W. J., W. E. Rodgers and E. L. Knuth, "Scattering of Argon Beams with Incident Energies up to 20 eV from a (111) Silver Surface," J. Chem. Phys. 56:1652-1657, 1972.

5. Liu, S. M., W. E. Rodgers and E. L. Knuth, "Interactions of Satellite-Speed He Atoms with Solid Surfaces," presented at the American Geophysical Union Fall Annual Meeting, San Francisco, Dec. 1971.

6. Liu, S. M., W. E. Rodgers and E. L. Knuth, "Transition between Atom-Surface Scattering Regimes," Advances in Applied Mechanics, Supplement 8, 2:E8-1 - E8-10, 1974.

7. Hays, W. J., "Scattering of Argon Beams with Incident Energies up to 20 eV from a (111) Silver Surface," School of Engineering and Applied Science, UCLA, Report No. UCLA-ENG-7061, 1970.

8. Liu, S. M., "An Experimental Study of Interactions of Hyperthermal Atomic Beams with (111) Silver Surfaces and Adsorbed Molecules," School of Engineering and Applied Science, UCLA, Report No. UCLA-ENG-7510, 1975.

9. Young, W. S., "An Arc-Heated Ar-He Binary Supersonic Molecular Beam with Energies up to 21 eV," School of Engineering and Applied Science, UCLA, Report No. 69-39, 1969.